1 Introduction

In most petroleum refineries, fluid catalytic cracking (FCC) unit is a primary conversion unit to produce light products such as gasoline, diesel oil and liquefied petroleum gas (LPG) from heavier feedstock such as vacuum gas oil (VGO) and vacuum residue (VR). To a large extent, the efficiency of their FCC units determines the profitability of many refineries. Since its invention in 1940s, a lot of efforts have been made to intensify the overall process to make it more efficient, reliable and profitable. [1-4] In recent decades, fast rising oil price, heavier and more contaminative feedstock, more stringent environmental regulations have made further FCC process intensification technologies more indispensable and important.

As an indispensable part of a FCC unit, a regenerator is used to burn off coke deposited on catalyst during reactions for catalyst activity restoration. Primarily, the carbon content in regenerated catalyst (CRC) is required to be 0.05~0.1 wt% or lower from ~1.0 wt% in spent catalyst. Otherwise, O_2 concentration flue gas is also required to be minimized to reduce air consumption and avoid possible afterburn. Finally, higher reaction rate, usually quantified by an index called by coke combustion intensity (CBI) defined as [5]

$$\mathrm{CBI} = \frac{\text{weight of coke burned (kg)}}{\text{time (h)} \times \text{catalyst inventory (ton)}}, \tag{1}$$

is required in a well-designed regenerator which requires smaller vessel volume and solids inventory. Finally, well-designed regenerators also provide an environment that preserves catalyst activity by restraining hydrothermal deactivation so that catalyst makeup is minimized. Therefore, it is desirable that less catalyst inventory and intermediate temperature are selected in a regenerator. From a view point of chemical reaction engineering, an ideal regenerator is a heterogeneous gas-solids reactor that demands high conversions of both gas and solids phases as well as high reaction rate in a mild environment.

There are two coke combustion modes practiced in FCC regenerator designs: incomplete and complete modes. In incomplete regeneration mode, a less-than-stoichiometric amount of air is provided to the regenerator. More CO and almost no O_2 are present in the flue gas. Less heat is released. Typically, an incomplete regenerator is designed to operate in a turbulent fluidized-bed reactor (usually referred as a single-stage regenerator) with a superficial gas velocity range of 0.6~1.2 m/s.[6] In an incomplete regenerator, the lower operating temperature and reductive atmosphere (due to the higher CO concentration) lead to higher catalyst-to-oil ratio and mild hydrothermal deactivation, resulting in better reactor yield, less makeup of fresh catalyst and less NO_x emission. Otherwise, less energy is consumed due to less air provided. However, there are drawbacks as well. First, it is difficult to burn coke cleanly in an incomplete regenerator. The vigorous mixing of solids in a turbulent fluidized bed makes the regenerator act like a continuously stirred tank reactor (CSTR), so that the exit CRC is nearly equal to the carbon content in the whole regenerator. Unless there is a very large catalyst inventory, it is difficult to achieve a low CRC. In a traditionally-designed incomplete regenerator, the typical CRC ranges from 0.15 wt% to 0.20 wt%.[7]

In contrast, excess air is provided to a regenerator operated in complete regeneration mode, thus resulting in almost no CO in flue gas. O_2 concentration in flue gas is typically in the range of 1.0~3.0 v% on a dry basis,[8] much greater than in an incomplete regeneration mode. A two-stage design is typically adopted in a complete regenerator where at least two regeneration zones or vessels are operated in series with either cascading or separate flue gas trains. The first stage operates in low-temperature incomplete regeneration mode and the second stage operates in high-temperature complete regeneration mode where less water steam exists and additional air is introduced. It is easier to realize lower CRC in complete regenerators than a single-stage incomplete regenerator, but they are mechanically more complex, more expensive in device manufacture, more difficult to operate and more energy-consumptive.[9]

Is there a solution to regenerate catalyst cleaner while still operated in incomplete regeneration mode? The answer is probably yes. A modification of the single-stage regenerator by adding suitable internal baffles in the dense bed can achieve staged regeneration in a single vessel (SRSV), resulting in cleaner regenerated catalyst equivalent to in a two-stage regenerator. Properly designed baffles in fluidized beds can strengthen gas-solids contacting by breaking up bubbles and improving lateral bubble distribution and narrow residence time distributions of both solids and gas by suppressing their axial backmixing. These effects of baffles helps to accomplish cleaner regenerated catalyst and higher CBI in FCC regenerators.

KBR proposed RegenMax technology[9,10] based on assemblies of packing internals (see Fig. 1) in a single fluidized-bed regenerator as shown in Fig. 2. Compared with a fluidized bed without baffles, the internal solids circulation flux across the baffle section in the baffled bed was found to be reduced by 81% in cold model experiments. Its effects on regeneration performance were further confirmed by Sapre's regenerator model.[11] The modeled results showed that RegenMax operated in partial combustion mode could also achieve the same CRC as in a two-stage regenerator without increase in catalyst inventory.[9]

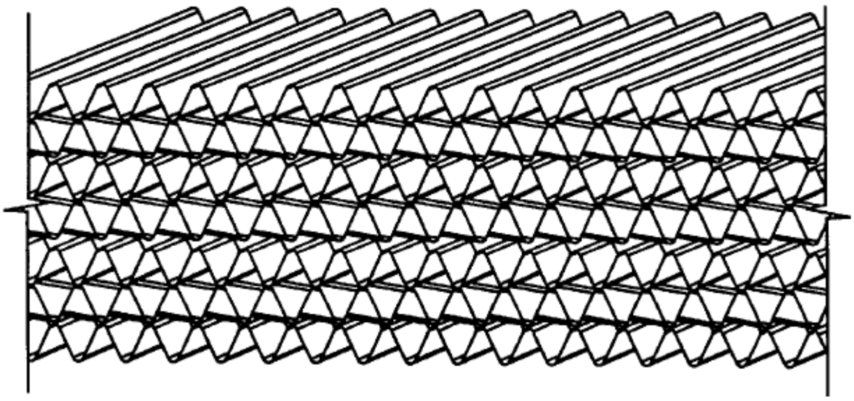

Fig. 1 Packing baffle in USP 6,503,460 [10]

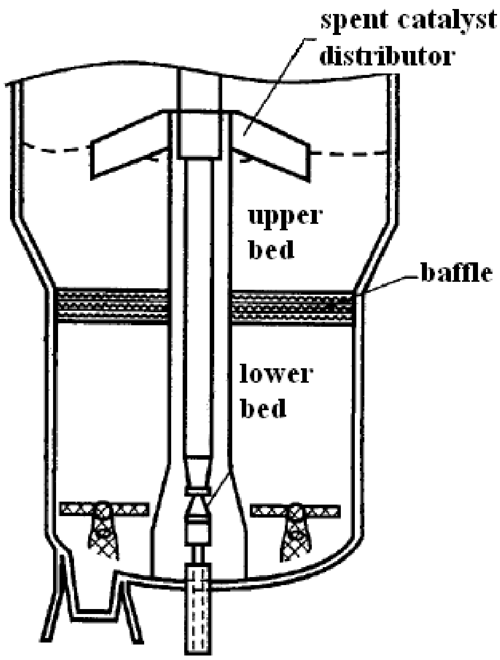

Fig. 2 Schematic of the RegenMax technology [10]

As an effective aid in fluidized-bed reactors, the effects of internal baffles in fluidized beds have attracted a lot of attentions in both academic and industrial communities. Baffles have already been successfully applied in fluidized reactors of phthalic anhydride, acrylonitrile,[12,13] vinyl acetate,[14] FCC spent catalyst strippers[15,16] to promote conversion, productivity, product selectivity and recovery, etc. Reviews on the effects of baffles in fluidized beds have been provided by Harrison and Grace and Jin et al. [17,18]

Except for reports of RegenMax technology,[9, 10] there are still few systematic studies on baffle's effects on a turbulent fluidized bed like a single-stage FCC regenerator. Zhang et al.[19] reported the performances of FCC regenerators with two layers of mesh-grid baffles. Reduced CRCs and increased CBIs were achieved indicating baffle's effect to improve catalyst regeneration. Hedrick proposed a three-stage counter-current FCC regenerator in a recent patent,[20] where, similar as the RegenMax technology,[9, 10] partial combustion regeneration was adopted to provide mild environment for catalyst activity protection and the staging effect of baffle was used to burn catalyst cleaner. The major difference is two layers of baffle employed which enables three regeneration sections of different operating temperature, namely calcination section, gasification section and combustion section in the dense bed. In a small pilot plant of diameter 50 mm I.D., Li et al.[21] examined the performance of a multi-stage countercurrent regenerator. Under same partial combustion conditions, the conversion of NO was increased to 90% in a multistage regenerator as compared to 50% in a single stage regenerator. Moreover, the CRC was reduced to 0.02 wt% as compared to 0.28 wt% in a single stage regenerator. The effect of adding baffles to reduce CRC in a regenerator could also be proved by the modeling work by Guigon et al.[22] They established a multistage FCC regenerator model based on Kunii-Levenspiel fluidized bed model and found that a multistage regenerator is superior to a single-stage regenerator in lower CRC.

Despite of these studies, deep understanding of baffle's effects on the hydrodynamics, mass transfer and gas/solids mixing of a turbulent fluidized bed like a FCC regenerator is still lacking. Moreover, the inner mechanism in a baffled turbulent fluidized bed that contributes to the enhanced regeneration performance is still not well known. In this study, we proposed a multilayer baffle for FCC regeneration intensification.[23] A large three-dimensional (3-D) cold model of 0.8 m I.D. was built to measure the effects of the new baffle on bed hydrodynamics, mass transfer and solids mixing quantificationally. These data were further incorporated in a baffle-free regenerator model [24] to predict the potential effects on regenerator performance.

2 Idea of the novel baffle

The idea of the new FCC regeneration intensification baffle came from a series of fundamental experimental studies in a two-dimensional (2-D) cold model.[25-29] Based on these research results, a new baffle system is proposed which aims to enhance gas-solids contacting and suppression of solids backmixing in large commercial turbulent fluidized bed reactors. This baffle is a type of multilayer internal. Figure 3 shows a schematic top view of one layer of this new baffle system for a vessel of circular cross-section. As seen in Fig. 3(a), multiple parallel flow regions are defined by vertical partitions. In each flow region, multiple inclined vanes are mounted in parallel to the partition, as shown in Fig. 3(b) from a section view of A-A plane in Fig. 3(a). In Fig. 3(a), each hatched block represents an inclined vane, where the thick and thin short lines perpendicular to the partitions represent the top and bottom edges of the vane, respectively. Otherwise, the vane angles in two adjacent flow regions are opposite. Each flow region can be viewed as a piece of louver baffle, so the whole layer shown in Fig. 3(a) is actually a combination of multiple louver baffles with interlaced vanes in every adjacent pair.

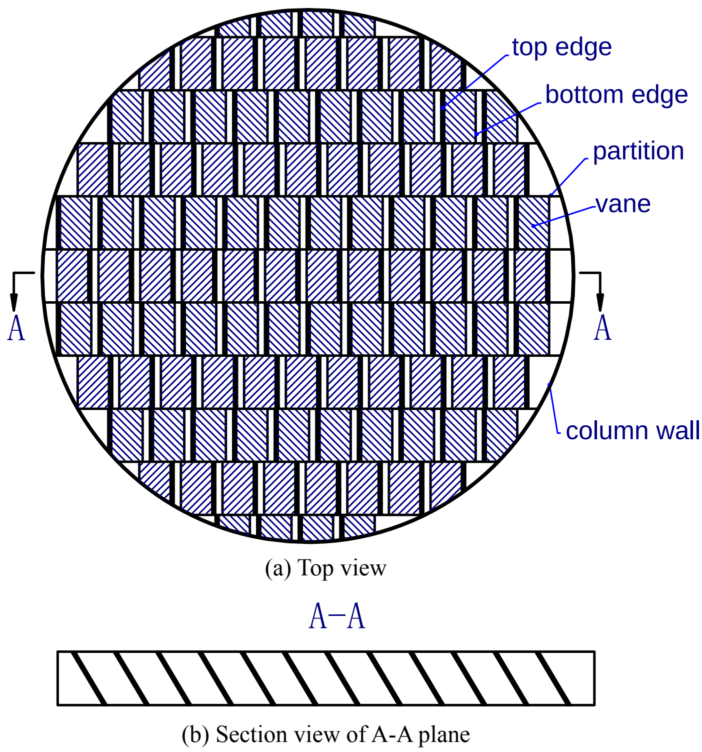

Fig. 3 Schematic of the new baffle for fluidization columns of circular cross-section

In this baffle configuration, the flow of gas and solids adjacent regions can generate interlaced contacting above and below a baffle layer, causing stronger local turbulence in gas and solids flows. This promotes further bubble splitting and strengthens gas-solids contacting. As indicated by a previous study,[27] when a relatively small bubble passes through louver baffles, parts of the bubble split by the vanes tend to coalesce and form a new bubble without significant change in its size. However, due to the opposite vane angles in adjacent flow regions in the new baffle, the broken parts of a bubble in different flow regions tend to be directed in opposite directions, making coalescence more difficult. Therefore, this structural configuration is more favorable in breaking bubbles and strengthening gas-solids contacting. This configuration can also limit the scale of internal emulsion circulation observed in fluidized beds with louver baffles[27] and distributing gas flow more uniformly over the bed cross-section.

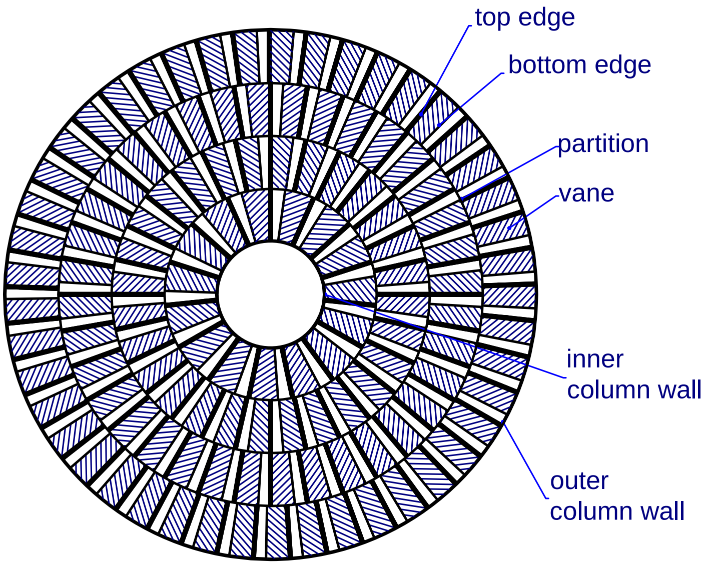

Fig. 4 Schematic of one layer of the new baffle for columns of annular cross-section

The baffle configuration shown in Fig. 3 could also be applied to columns of circular cross-section, e.g. the regenerator of a KBR Orthoflow FCC unit.[30] Figure 4 shows the baffle's configuration for columns with annular cross-section. Several concentric annular flow regions with vanes of opposite vane angles are mounted in adjacent pair flow regions to promote improved gas-solids contacting.

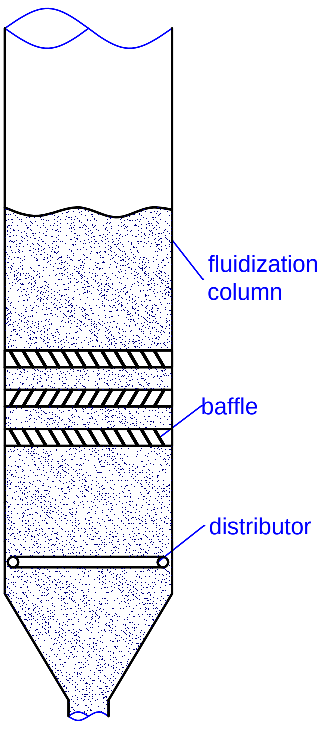

Fig. 5 Arrangement of the new baffle in a turbulent FCC regenerator

Vertically, multiple layers of the new baffle installed in a turbulent FCC regenerator can be arranged as shown in Fig. 5. The spacing between adjacent pairs of baffle layers is relatively small, usually 1 to 3 times of the baffle layer height. Flow regions between each pair baffle layer are of similar geometry, but with opposite vane angles, similar arrangement as in the 2-D column of our previous studies.[26, 28, 29] As demonstrated previously, this arrangement can further strengthen gas-solids contacting in the bed. In a single stage FCC regenerator, the new baffle should be arranged as in Fig. 5 with several layers of baffles in the middle of the bed to divide the fluidized bed into two stages. Unlike a FCC packed stripper, a regenerator only needs limited solids backmixing suppression to avoid too large axial temperature gradient, otherwise very low-temperature zones are possible to appear, resulting in low coke combustion rate and impairing the regenerator performance as a whole.

By now, a China patent [23] has been granted to this baffle idea described above. Recently, we also used this baffle in a binary fluidized bed with FCC particles (Geldart A) and millet (Geldart B).[31] Due to the baffle's enhancement on gas-solids contacting and suppression on solids axial dispersion, enhanced particle segregation was observed. The gas velocity range suitable for particle classification was also broadened in a baffled fluidized bed, which made it a potential high-efficiency continuous particle classifier.

3 Large-scale cold model experiments

3.1 Experimentation

In order to minimize the scale-up effect between experimental and industrial unit, a large-scale cylindrical fluidized-bed column of 800 mm I. D. as shown in Fig. 6 was employed. According to the study of Werther,[32] a critical minimum column diameter of 0.5 m was recommended for scaling-up fluidized beds of fine Geldart A particles. Further increase in column diameter than 0.5 m does not add significant scale-up effects. The height between the gas distributor and cyclone inlet was about 11 m. A sparger gas distributor, the same type distributor as in industrial FCC regenerators, was utilized in the cold model. The open area ratio of the distributor in the column was 1.95%. A cyclone on the top of column captured the entrained particles and returned them to the bed via a dipleg to ensure a constant particle inventory in the bed.

Equilibrium FCC particles and compressed air were used in this study as fluidizing solids and gas, respectively. Detailed properties can be referred in Table 1. The solids inventory was kept constant in all conditions. In the baffle-free fluidized bed (FFB), the static height in the column was maintained at 1.9 m. After adding the baffles, there was an indiscernible increase in static height. The superficial gas velocity ranged from 0.17 m/s to 0.98 m/s, covering both the bubbling and turbulent flow regimes.

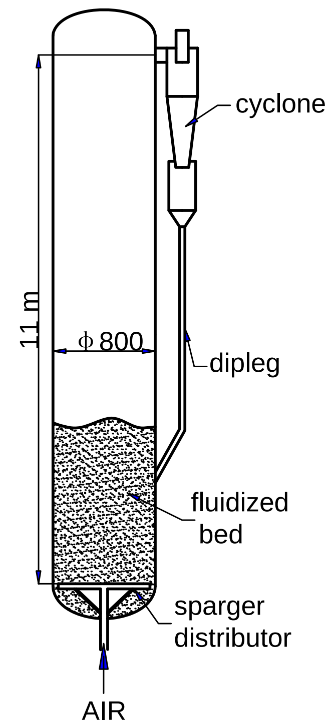

Fig. 6 Schematic of the 3-D cold model column

Table 1 Major property of the employed particles

Item	Value
Mean diam., μm (spec. surf. area)	81
Particle density, kg/m^3	1500
Bulk density, kg/m^3	917
F_{45}	0.066
u_{mf}, m/s	0.0049
ε_{mf}	0.43

There were 29 pressure taps mounted on the cold model column wall to measure the absolute pressures and differential pressures between adjacent taps to obtain the axial profiles of particle concentration and properties of pressure fluctuations. Each pressure tap was a steel tube of 6 mm I.D. Wire gauze was inserted into the tips of pressure taps to prevent entry or blockage of fine particles. For all pressure measurements in this study, the dead volumes of all pressure transducers were maintained to be less than 8000 mm^3 to avoid damping of pressure signals.[33] The absolute pressure transducers used in this study were Gems-1200. The differential pressure transducers were CYB020K and CYB050K from Tianshui Huatian Microelectronics Co., LTD with ranges of 20 kPa and 50 kPa, respectively. The analog signals from transducers were converted into digital signals by an ADLINK PCI9111-DG A/D converter and then saved in a computer. The sampling frequency was 200 Hz and sampling interval was 60 s for all runs.

A homogeneity index based on bed expansion [34] and a heterogeneity index based on differential pressure fluctuation were utilized to character the gas-contacting or the fluidization quality in the fluidized bed. Actually, this homogeneity index represents the extent to which an actual fluidized bed approaches its ideal state of homogeneous fluidization, i.e. with best fluidization quality. Detailed description on the definition of this index and the method for its calculation can be referred in one of previous publications.[34] The heterogeneity index was based on the study of Roy and Davidson[35] who found that the amplitude of differential pressure fluctuations measured across a small axial internal of the bed was proportional to the bubble size, with bubble size estimated from the equation of Darton et al.[36] Later, the analysis by Bi [37] and Zhang et al.[38] further demonstrated that differential pressure signal across a small axial internal can filter out more global compression waves that are irrelative to bubble size while keep more localized bubble-related waves. In this study, the pitches between two pressure taps in the dense bed were all maintained to be smaller than 300 mm. Furthermore, the measured differential pressure signals were processed with a band-pass filter to keep the signals in the frequency range of 0.2−40 Hz to filter out signal components due to gas flow-rate fluctuations and noises.[39] The processed differential signals will be more suitable to characterize the gas-solids contacting quality in the bed. Therefore, the average of their standard deviations in the dense bed, i.e.

$$I_{\mathrm{hetero}} = \overline{\sigma_{\mathrm{dp}}}\,, \tag{2}$$

was used as another fluidization quality index called heterogeneity index in this study. Note here, I_{hetero} is dimensional and with the same unit with pressure while the homogeneity index, I_{homo}, is dimensionless.

In order to study the effect of baffles on gas backmixing, a steady-state tracer technique was employed in this study. As shown in Fig. 7, hydrogen as tracer gas was continually injected downward through a point injector located on the column axis and 1.36 m from the bottom gas distributor. The flow rate of tracer gas was set at 1% of the flow rate of fluidized air at all gas velocities. Gas was sampled at 28 taps below the injector with different distances from the injector and at different radial positions. In order to sample from different radial positions simultaneously, 4 specially designed sampling tubes as shown in Fig. 8 were employed. Each tube had 7 sampling taps distributed evenly along the bed radius. In order to minimize errors due to the disturbance of the sampling tubes on gas-solids flow in the bed, the seven sampling gas intakes were all located on the side surface of the sampling tube. The main sampling tube was a steel tube with 20 mm I. D. and the hoses connecting the sampling tabs were $\phi 3\times 1$ mm plastic tubes. Wire gauze was inserted into the tips of sample tubes to prevent blockage of particles. According to the different rows and columns, sampling taps were named A1-A7, B1-B7, C1-C7 and D1-D7. Figure 7 gives the positions of all the sample taps (all lengths with units of millimeter). There was also another sampling tap mounted at the gas outlet tube of the 3-D column to measure the tracer gas concentration in the freeboard. In experiments, sampling gas automatically flowed into the two-liter sampling bags due to the positive pressure in the bed. The sampling interval of every test was about 15~20 minutes to benefit obtainment of repeatable data. A gas chromatograph with TCD detectors was utilized in this study to measure the tracer gas concentration of the sampled gas.

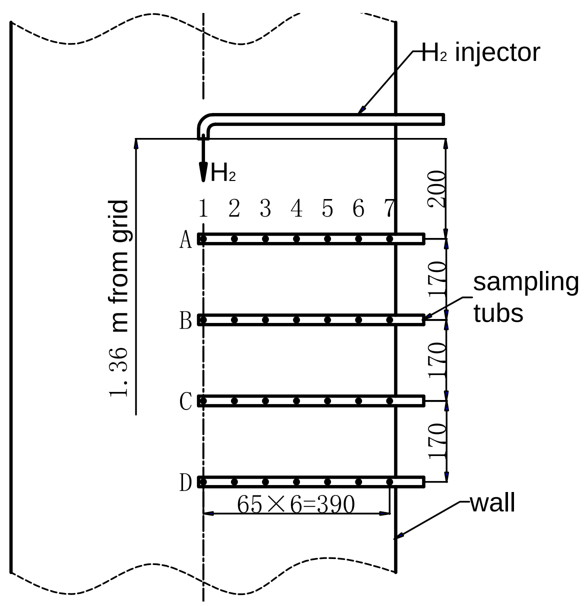

Fig. 7 Steady-state tracer experimental setup in the 3-D column (all dimensions in mm)

In fluidized beds of fine Group A particles, solids mixing and gas mixing are closely related. Especially, gas backmixing is predominantly affected by the entrainment of solids due to their macro circulation in the bed, i.e. the so-called "gulf streaming".[29,40-42] Due to various limitations, studying solids bacmixing in fluidized beds using solids tracers is very difficult and repeatable solids dispersion results are more difficult to obtain.[29] As an approximate approach, we utilized the results from steady gas tracing experiments to quantify the baffles' effects on suppressing solids backmixing in this study.

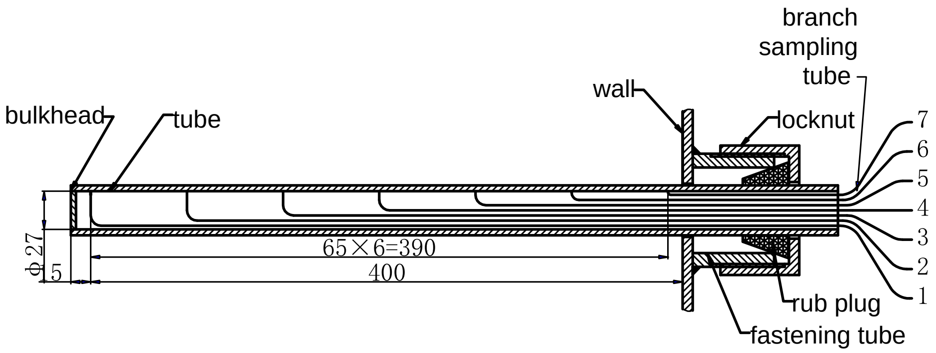

Fig. 8 Gas sampling tube used in the 3-D column (all dimensions in mm)

Except for experiments on gas-solids contacting and gas/solids backmixing, particle carryover fluxes were also measured to investigate the effects of baffles on particle carryover. A butterfly valve was installed in the dipleg of the cyclone separator. By measuring the time needed for the cyclone separator to fill a volume of 3.77 liters, the particle carryover flux was determined. In most cases, more than ten measurements were carried out for each operating condition to assure the repeatability and reliability of experimental results.

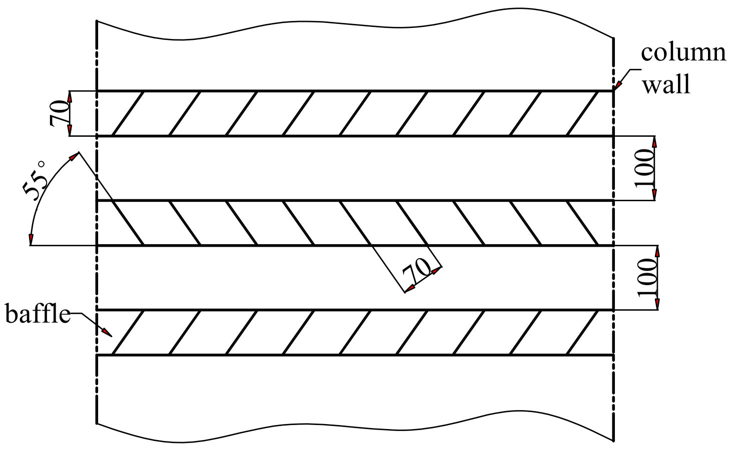

Fig. 9 Baffle arrangement in the fluidized-bed column (all dimensions in mm)

Based on our previous studies,[25-29] three layers of new baffles were designed and installed in the fluidized-bed column, as shown in Figs. 9 and 10, where flow regions in adjacent pair layers were parallel with opposite vane angles. This is a similar arrangement as our previously studied baffle structure in 2-D columns.[26, 28, 29] It had same vane pitch, vane angle and baffle layer height as our optimized baffle structures in our 2-D experiment. The heights (distance from the bottom of each baffle layer above the gas distributor) of the three baffle layers were 0.7 m, 0.87 m and 1.04 m. The spacing between adjacent pairs of baffle was 100 mm, a little larger than the height of the baffle (70 mm). The vane pitch was 70 mm and the vane angle was 55^{o}. Figure 10 shows the photograph of one layer of the new baffle employed in this study. There were 10 parallel flow regions in each baffle layer. The width of flow region was 70 mm, comparative to the vane pitch. For each of the five partitions, there were two rows of vanes of opposite vane angles welded on its two sides. This was to reduce the resistance to gas or solids flow through the baffle layer. The vertical partitions were made of 5 mm steel plates, whereas the vanes were fabricated from 3 mm steel plates. The whole layer of baffles was fixed by welding the five partitions to the inner steel wall of the column. The interlaced junctions of the vanes in adjacent pairs of flow regions were also welded together to strengthen the baffle layer. Except for the baffled fluidized bed (BFB) studied, a baffle-free fluidized bed (FFB) was also studied with respect to its hydrodynamics and gas/solids backmixing properties to facilitate understanding the effects of the new baffle.

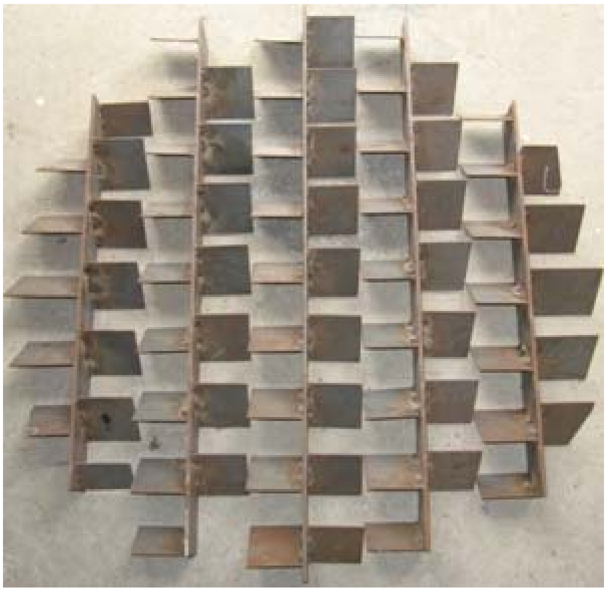

Fig. 10 Photograph of one layer of the new baffle

When carrying out gas-tracing experiments, the arrangement of baffles and sampling tubes are diagrammatically shown in Fig. 11. The three layers of new baffles were mounted between adjacent pairs of tracer sampling tubes. Moreover, the arrangements of the sampling tubes and gas injector were the same as for FFB.

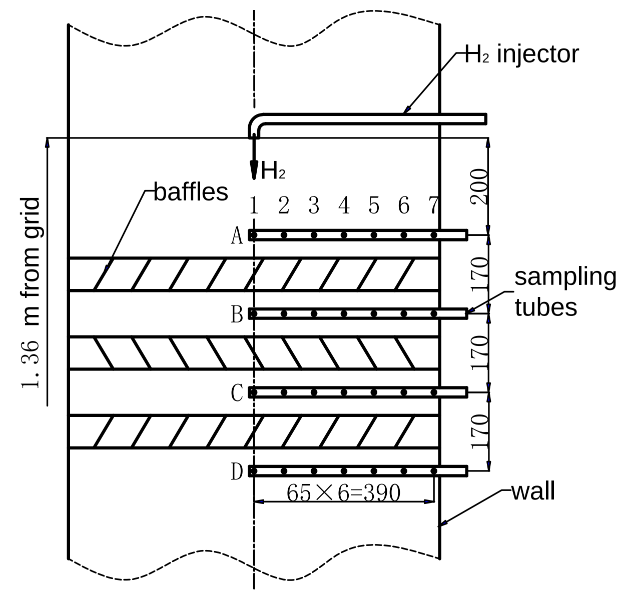

Fig. 11 Configuration of new baffles and tracer sampling tubes (all dimensions in mm)

3.2 Experimental results and discussion

3.2.1 Effects on gas-solids contacting

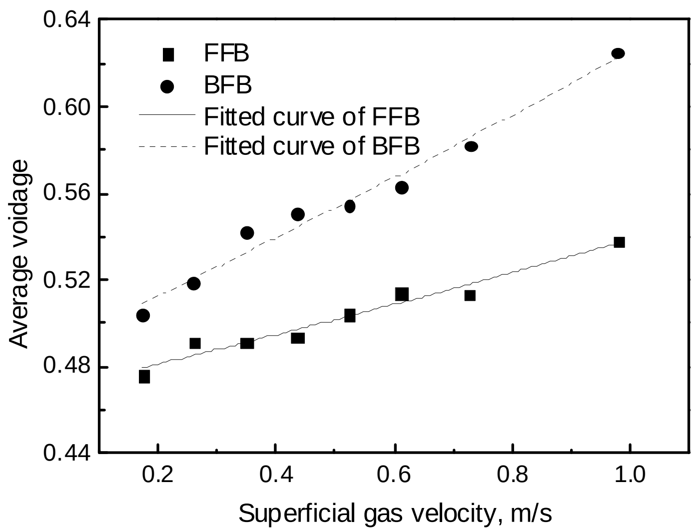

Fig. 12 Comparison of average voidage

Figure 12 compares the average voidages determined by differential pressure measurement in the FFB and BFB. A significant increase in bed expansion is observed after installation of the new baffle. As bed expansion in a fluidized bed is primarily determined by bubble properties, i.e. bubble size and rise velocity, the significant increase in bed expansion due to insertion of the new baffle indicates a noticeable improvement in bed fluidization quality or gas-solids contacting.

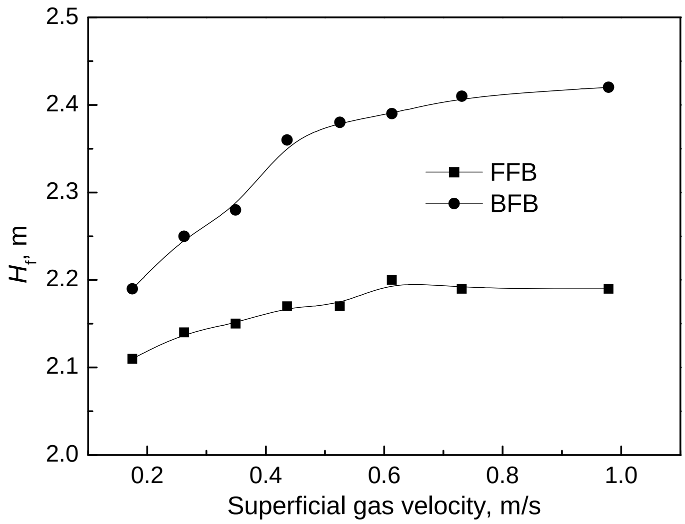

Fig. 13 Comparison of expanded bed heights

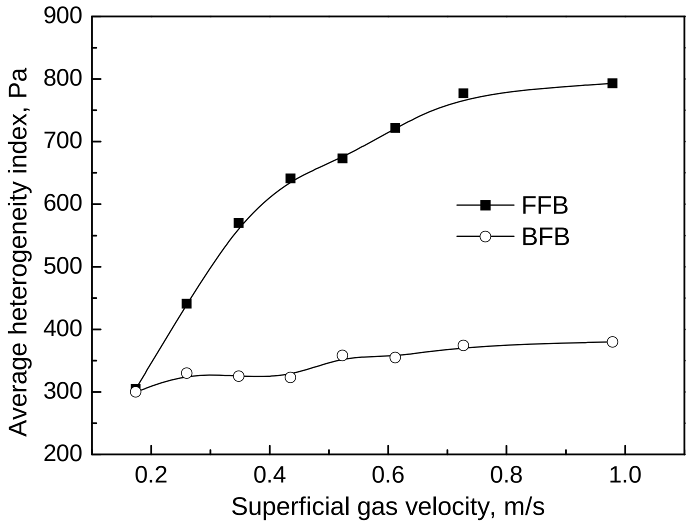

Fig. 14 Comparison of heterogeneity indices of FFB and BFB

The higher bed expansion can also be observed in Fig. 13 where the expanded bed heights of FFB and BFB, obtained by the method proposed in Zhang et al.[43] based on the abrupt decrease in the amplitude of pressure fluctuations across the dense bed surface, are compared. Again, the bed height is always larger after baffle insertion. The difference increases with increasing superficial gas velocity. Unlike in smaller laboratory-scale fluidized beds, the measured bed height in the large column of this study first increased and then decreased slightly at $u_0 \approx 0.6$ m/s. This is due to the fast increase of particle inventory in the large-volume freeboard which suppresses the increasing bed expansion due to increased gas velocity.[43] Due to the same reason, the bed height increase rate in BFB also shows a remarkable decrease after u_0 > 0.6 m/s. However, its bed height continues to increase after u_0 >0.6 m/s, a different trend from in FFB, which indicates the baffle's stronger effect on retaining bubbles in bed.

The higher bed expansion in BFB is closely related to the hydrodynamic changes caused by the baffles inserted. Figure 14 compares the average heterogeneity indices, I_{hetero}, defined by Eq. (2), of FFB and BFB. Clearly, BFB has lower I_{hetero}s than FFB, especially under high superficial gas velocities. As discussed earlier, I_{hetero} follows a monotonic increase with increasing average bubble diameter. Therefore, it can be inferred from Fig. 14 that the average bubble size is greatly reduced.

It is noticeable that, as an index indicating the fluctuation amplitude of the processed differential pressure signal, I_{hetero} of FFB in Fig. 14 does not shown a peak with increasing gas velocity that was often seen in small laboratory-scale fluidized beds.[44-48] The corresponding superficial gas velocity to this peak is usually defined as the onset gas velocity of turbulent flow regime.[48-50] The gas velocity range in this study was large enough to cover the onset gas velocities of turbulent regime predicted by the widely accepted correlations.[45, 51, 52] Why there existed such a different trend of pressure fluctuation in this study? The recent studies on deep fluidized beds by Well,[53] Karri et al.[54] and Issangya et al.[55] may give the answers. In their studies on fluidized beds of Geldart A particles, they found a phenomenon called "gas streaming" happened when static bed heights were high. This is a serious gas bypassing near the column wall with high rise velocities, resulting in poor gas-solids contacting in bed. They attributed "gas streaming" to the resultant defluidization of some zones in the bed bottom due to the gas compression by high bed pressure drops. In a deep fluidized bed with "gas streaming", Karri et al.[54] also found a monotonic increase of pressure fluctuation with increasing superficial gas velocity, which was in agreement with the results in Fig. 14. In large-scale fluidized beds such as industrial reactors, it is expectable that gas distributors are more difficult to distribute the gas flow as evenly as in small-scale beds. Gas in fluidized beds always seeks the lowest resistance path to the bed surface, so bubbles coalesce more readily, leaving regions with less bubble flow. These areas are easier to deaerate or even defluidize than in small-scale fluidized beds. Overall, "jet streaming" is a combined result from gas compression, imperfect gas distribution and scale-up effect.

Later, Issangya et al.[55] found that adding mesh-grid baffles or add more fines in bed could effectively eliminate or suppress "gas streaming" at least. In our study, the fine content was much smaller than the operating need in industrial FCC units (~20 wt%) [5] and the static bed height was high. It is then expected that "gas streaming" was very possible in FFB. The effect of baffle on suppressing "gas streaming" can also be seen in Fig. 14 as indicated by the lower heterogeneity indices in BFB. In view of Cocco et al.,[56] baffles causes the less permeable solids to separate as the solids flow around them, which helps expose more catalyst surface area, allowing gas to permeate into solids and making gas easier to aerate the solids and prevent defluidization.

Except for suppressing "gas streaming", the high bed expansion in BFB can also be related to the baffle's effect on improving the gas distribution in the bed section. Non-uniform flow is an inherent characteristic of gas–solids fluidization systems, further aggravated in large-scale columns. With the aid of baffles, flow uniformity can be improved.

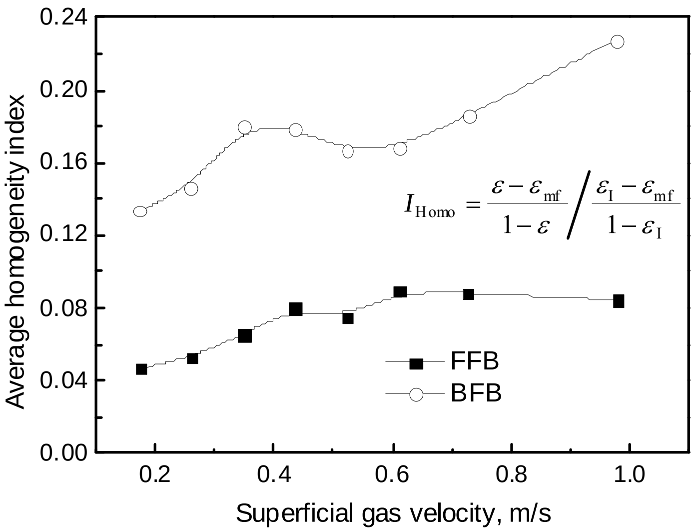

Fig. 15 Comparison of homogeneity indices in FFB and BFB

With this bed-expansion-based homogeneity index,[34] the baffle's improvement on gas-solids contacting can thus be quantified and compared as shown in Fig. 15. It is shown that the homogeneity indices of BFB are much greater than in FFB, usually 2~3 times those of FFB, also inferring a pronounced improvement in gas-solids contacting and fluidization quality.

3.2.2 Effects on gas/solids backmixing

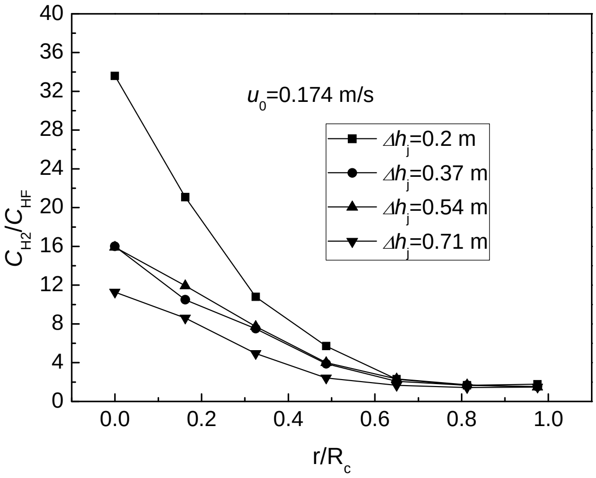

(a1)

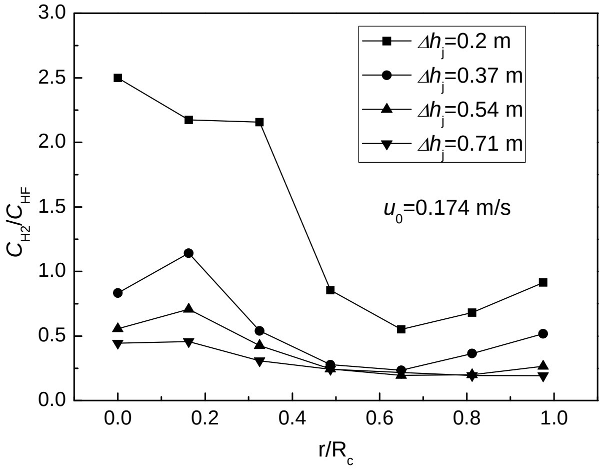

(b1)

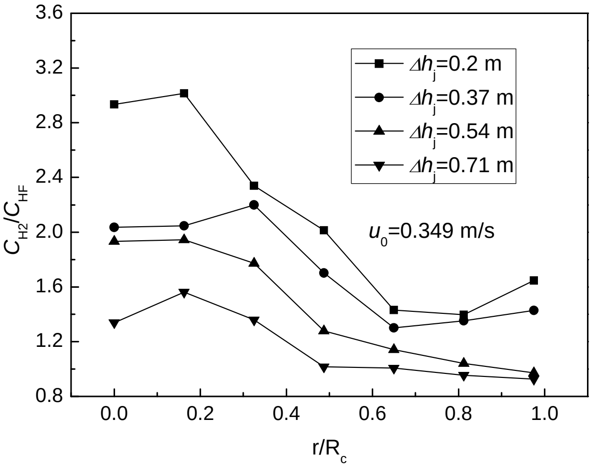

(a2)

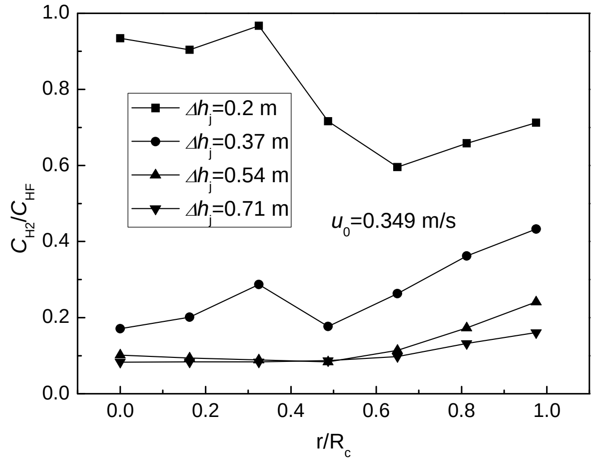

(b2)

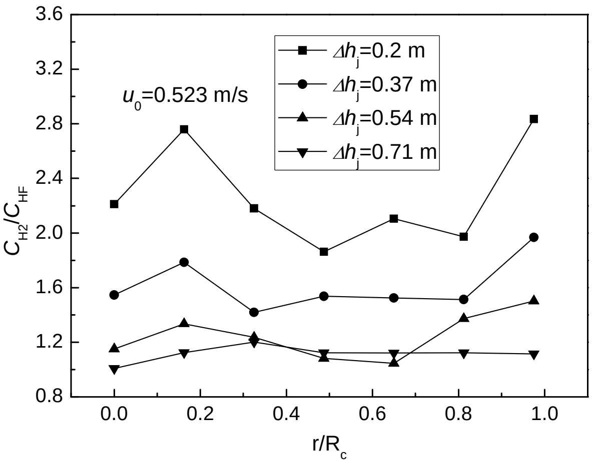

(a3)

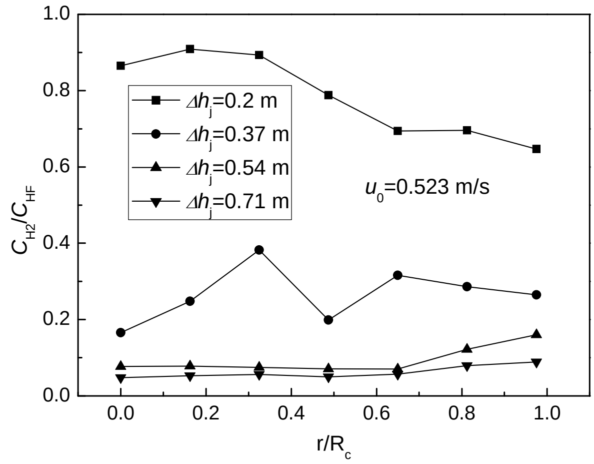

(b3)

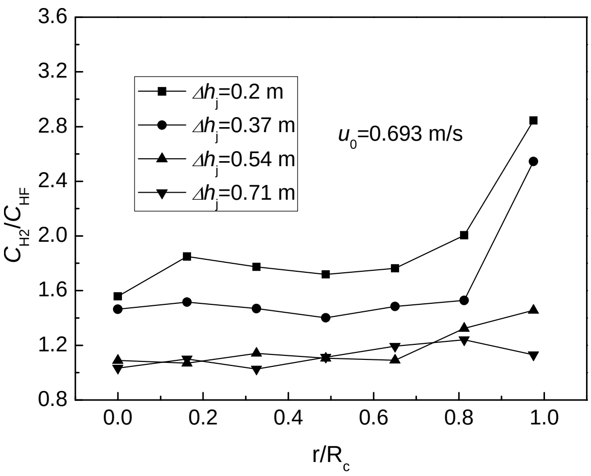

(a4)

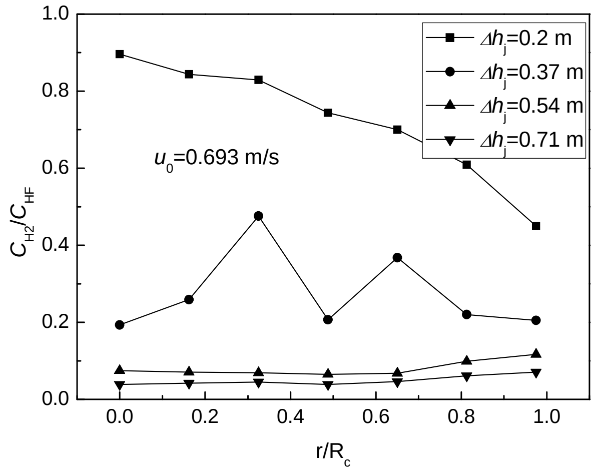

(b4)

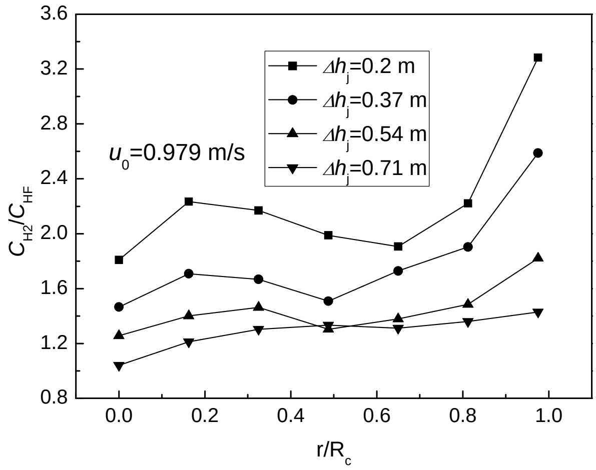

(a5)

FFB

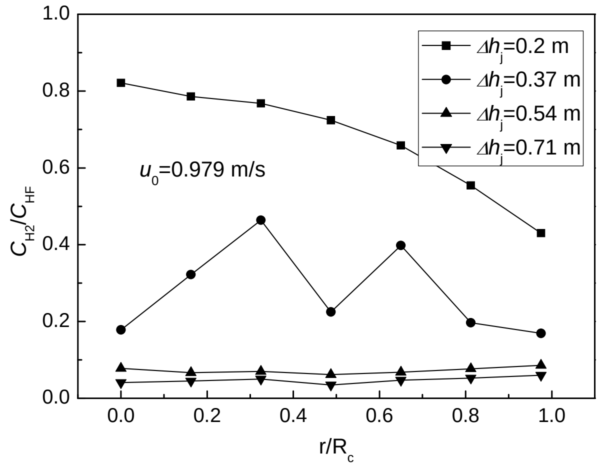

(b5)

BFB

Fig. 16 Tracer gas concentration profiles in FFB and BFB

Figure 16 compares the measured tracer gas (H_2) concentration profiles in the FFB and BFB of this study. On the one hand, it can be observed that, the backmixed tracer gas concentrations below the injector in FFB are much larger than those in BFB under same gas velocities, approximately in the range of 2~15 times. First, this reveals stronger gas/solids mixing in FFB. The stronger gas/solids mixing is strongly related to low fluidization quality in FFB, i.e. the gas bypassing, gas mal-distribution etc as discussed previously. Especially at u_0=0.174 m/s, the high H_2 concentrations and the large radial H_2 concentration gradients as shown in Fig. 16(a1) further demonstrate a very bad fluidization condition. In this condition, the sparger gas distributor cannot function well due to the low pressure drop, which may result in serious gas mal-distribution in the cross section of the dense bed. Otherwise, “gas streaming” due to the large static bed height and small fine content in this study leads to further worsening of the fluidization quality. On the other hand, the big differences in upstream tracer gas concentration reveals baffle's strong suppression on axial solids mixing. Detailed explanation on the mechanism of baffle's suppression on solids backmixing can refer to our previous publications.[27, 28]

By observing the tracer gas profiles shown in Figs. 16(a1)-16(a5), a transition of internal emulsion circulation pattern (i.e. the so called "gulf streaming")[57] in FFB can be found. As tracer gas concentrations primarily reflect the intensity of solids backmixing flux in a fluidized bed of fine FCC particles, these tracer distributions indicate that, at u_0 =0.174 m/s, most emulsion flows downward in the core region, while most bubbles rise outside this core region as seen in Fig. 16(a1). The near-wall regions with very low H_2 concentrations may still in defluidization. This emulsion flow pattern is commonly encountered in large fluidized beds with aspect ratio (h_f/d_t) close to unity.[57] As u_0 increases, the tracer concentrations near the wall became higher and higher, while they become lower and lower in the core region, indicating a transition of the emulsion circulation flow pattern in the bed. During this transition, bubble flow gradually occupied the downward flow area of emulsion in the core region, resulting in continuous increase in the downward flux of emulsion near the wall. When u_0 exceeded 0.693 m/s, the tracer gas concentrations near the wall were predominantly higher than in the core region (see Figs. 16(a4) and 16(a5)), indicating an up-centre & down-annulus emulsion flow pattern commonly observed in high-velocity large-scale fluidized beds and most small laboratory-scale fluidized beds.

Baffle's effect on suppressing solids backmixing can also be observed by comparing the derived axial gas dispersion coefficients in FFB and BFB from a one-dimensional steady dispersion model,

$$\frac{u_0}{\varepsilon}\frac{\partial C_{\mathrm{H2}}}{\partial z} = D_{\mathrm{a,g}}\frac{\partial^2 C_{\mathrm{H2}}}{\partial z^2} \tag{3}$$

Herein, C_{H2} is the area-averaged H_2 concentration at a certain height. Detailed procedure of deriving $D_{a,g}$ can refer to Zhang et al.[28]

Figure 17 compares the axial gas dispersion coefficients in FFB and BFB. Clearly, $D_{a,g}$ decreases significantly after inserting the new baffles especially at high gas velocities. This further proves the baffle's strong suppression on gas/solids backmixing. For further discussion, the gas dispersion coefficients measured previously in 2-D columns [25, 28] are also plotted as shown by the two dashed lines in Fig. 17. The baffles employed in the 2-D column had similar geometrical parameters (e.g. vane angle, vane pitch, layer pitch etc) to the baffles used in this study. Although similar effect on suppressing gas/solids backmixing are observed, but baffle's effect is clearly not so remarkable as in the large-scale 3-D column of this study. In other words, baffle-free fluidized beds have very large scale-up effects, which makes it very difficult in designing industrial units.[58, 59] However, with properly designed baffles inserted, the scaling-up will be much easier as inferred by Fig. 17.

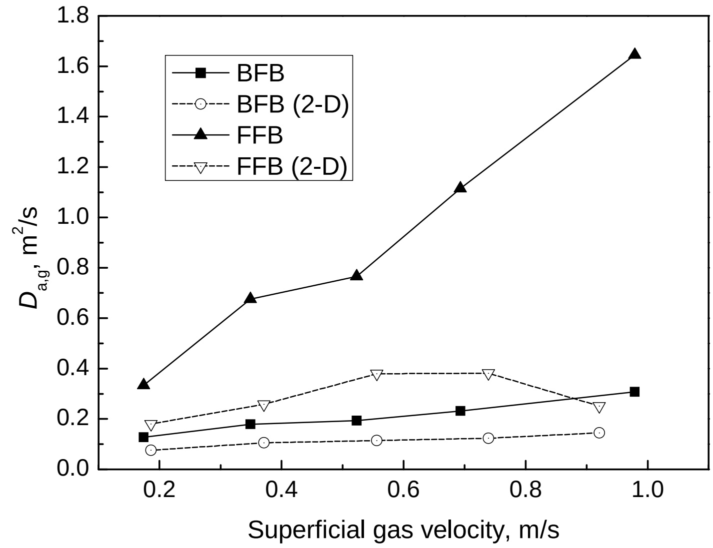

Fig. 17 Comparison of axial gas dispersion coefficients in FFB and BFB

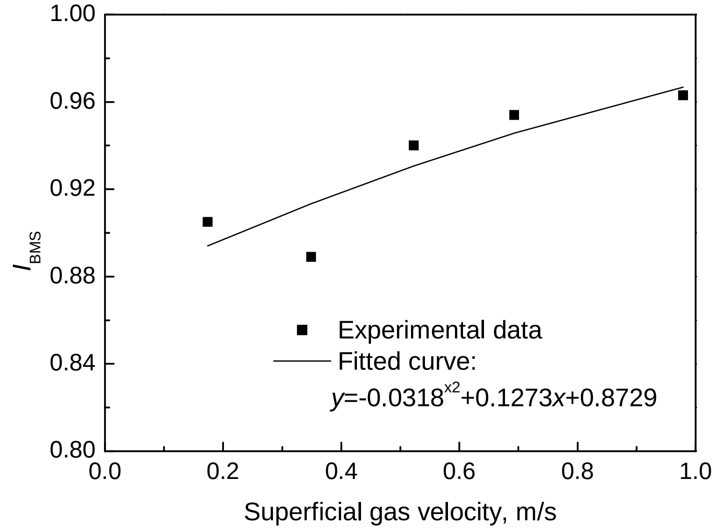

Fig. 18 Backmixing suppression index of BFB as a function of superficial gas velocity

If it is assumed that the downward drag by descending solids is the dominant cause of gas backmixing and the tracer gas concentration is proportional to the solids backmixing flux, a backmixing suppression index can be obtained by comparing the area-averaged tracer gas concentrations of FFB and BFB in Row D (see Figs. 7 and 11), i.e.

$$I_{\mathrm{BMS}} = 1 - \frac{\overline{C_{\mathrm{H2}}}\ \text{(@Row D in BFB)}}{\overline{C_{\mathrm{H2}}}\ \text{(@ Row D in FFB)}}. \tag{4}$$

As shown in Fig. 18, I_{BMS} is in the range of 0.89~0.96, indicating an 89~96% reduction of solids backmixing flux across the three-layer new baffles.

Compared to FFB, the much lower tracer gas concentrations and the more uniform radial distributions of tracer gas concentrations of BFB in Row A (see Fig. 16) indicate that: (1) the internal emulsion circulation above the baffle layers are also much weaker; (2) the new baffles can redistribute the gas flow, making it more uniform over the column cross-section. This is also agreeable with the results of gas-solids contacting.

3.2.3 Effects on particle carryover in freeboard

Table 2 Comparison of particle carryover fluxes in FFB and BFB

u_0 (m/s)	Particle carryover flux, kg/m^2.s		Net decrease (kg/m^2.s)	Relative decrease (%)
	FFB	BFB		
0.26	0.041	0.028	0.013	32
0.348	0.095	0.068	0.027	28
0.435	0.179	0.154	0.025	14
0.523	0.419	0.292	0.127	30
0.612	0.701	0.534	0.167	24
0.727	1.35	1.24	0.111	8
0.979	2.44	2.49	-0.050	-2

The carryover of particles in fluidized beds arises from two mechanisms: elutriation and entrainment.[57] Elutriation refers to the carryover of fine particles, with terminal velocities smaller than the gas velocity, by gas flow. Entrainment results from to the ejection of particles due to the eruption of bubbles at bed surface. Both large and small particles can be entrained into the freeboard. Some larger particles in the freeboard with terminal velocities greater than the gas velocity return to the bed after traveling a certain distance. Entrainment is strongly affected by bubble-related bed hydrodynamics. Larger average bubble size and more vigorous bubble eruptions at the bed surface contribute to stronger particle entrainment. In this study, baffles immersed in the bed influenced particle entrainment by changing the bubble behaviour.

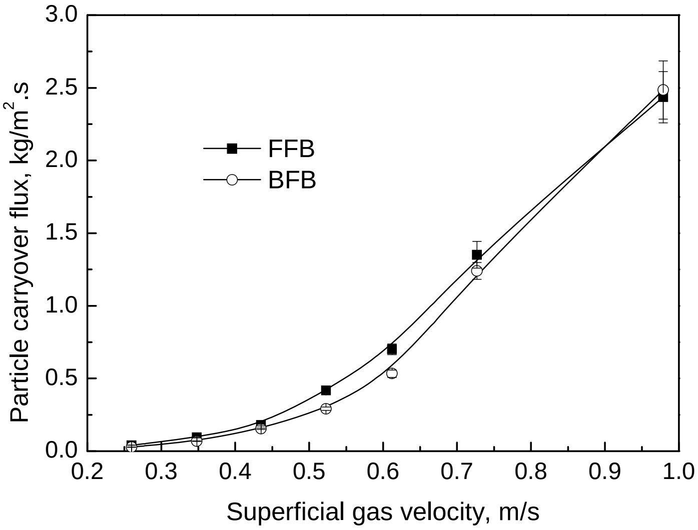

Fig. 19 Particles carryover fluxes in FFB and BFB

The particle carryover fluxes of FFB and BFB are compared in Fig.19 and Table 2. Clear reduction in particle carryover flux can be observed due to the baffles, even though the bed height of BFB is larger than that of FFB (see Fig. 13). The maximum reduction can be 30%. The reduction of particle carryover due to the baffles was more significant at relatively small superficial gas velocities. In such conditions, bubble behaviour may be the dominant influencing factor on particle carryover whereas baffle's effect on breaking bubbles is stronger.[27]

4 Baffle's effect on FCC regenerator performance

4.1 A counter-current baffled regenerator model

4.1.1 Introduction

In this section, the new baffle's effects on gas-solids contacting and solids backmixing were incorporated into a counter-current regenerator model [24] that we established recently to evaluate its effect on FCC regenerator performances. In this counter-current regenerator model, three-zone and two-phase gas model was utilized to describe the gas flow through the regenerator, addressing the different phase mass-transfer properties in the different zones. A new two-CSTR-with-interchange model was used to describe the solids flow and to address the effect of freeboard on catalyst regeneration. The model was programmed in Matlab language with coupled hydrodynamics and reaction kinetics models and tested and validated by the data from an industrial FCC regenerator operated under both partial and full CO combustion modes. The baffled regenerator model in this study follows similar model scheme except for the consideration of baffle effects. The model setup procedure also includes kinetics model, hydrodynamics model, mass balances of gas species and carbon and heat balance, similar to the baffle-free regenerator model.[24] For brevity, only different parts in the baffled regenerator model are described in the following contents. Details about other parts of this model can refer to Zhang et al.[24]

4.1.2 Model scheme

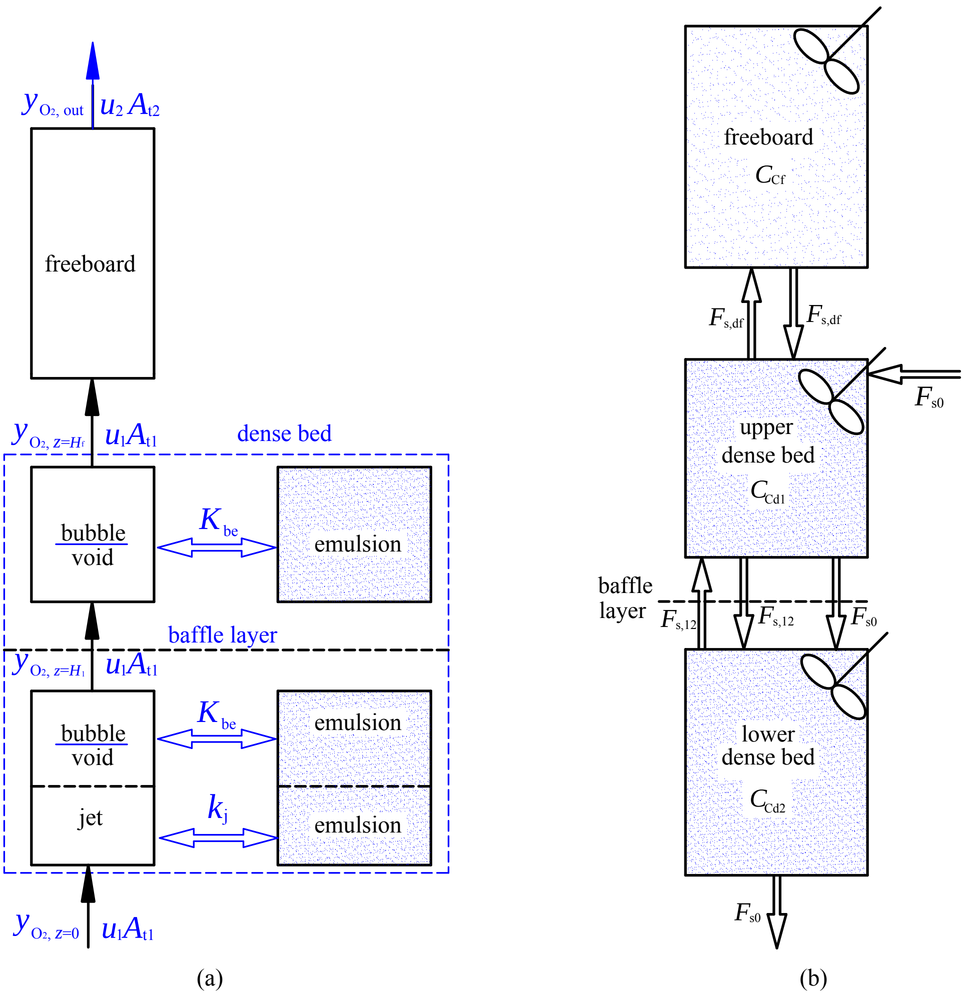

Fig. 20 Gas and solids flow patterns for the baffled regenerator model: (a) assumed gas flow pattern; (b) assumed solids flow pattern

For simplicity, effects on gas-solids contacting and solids backmixing are the two aspects of baffle effects considered in this baffled regenerator model. The gas and solids flow patterns are shown in Fig. 20. For gas flow pattern, the "two-phase bubbling bed model" proposed by Chavarie and Grace [60-62] is again used as shown in Fig. 20(a). This is almost the same as the baffle-free regenerator model.[24] The only difference lies in the interphase mass transfer coefficient, which is augmented due to the improvement of gas-solids contacting by the baffles. Due to the strong suppression of solids backmixing by baffles, solids flow through the dense bed is modeled as two CSTRs in series with an interchanging solids flux, $F_{s,12}$, as shown in Fig. 20(b). The freeboard is handled in the same manner as in the baffle-free regenerator model.[24]

4.1.3 Quantitative determination of the baffle effects

In this model, baffles effects on gas-solids contacting and solids backmixing suppression reflect the different interphase mass transfer coefficient, K_{be}, and the solids exchange flux across baffle layers, $F_{s,12}$, in the dense bed as shown in Fig. 20. In the following, the two parameters will be determined quantitatively based on our experimental results obtained in the large cold model.

(a) Interphase mass transfer coefficient in fluidized beds with new baffles

In this baffled regenerator model, the interphase mass transfer coefficient in the baffled regenerator is determined by comparing the measured average dense bed bubble fractions in BFB and FFB based on an interphase mass transfer coefficient correlation proposed by Sit and Grace:[63]

$$K_{be} = \frac{1.5u_{mf}}{d_b} + \frac{12}{d_b^{3/2}}\left(\frac{D_g \varepsilon_{mf} u_b}{\pi}\right)^{1/2}. \tag{5}$$

In view of the very small u_{mf} for FCC particles, Eq. (5) can be simplified to

$$K_{be} \approx \frac{12}{d_b^{3/2}}\left(\frac{D_g \varepsilon_{mf} u_b}{\pi}\right)^{1/2}. \tag{6}$$

For two fluidized bed operated at the same superficial gas velocities, this suggests that the ratio of K_{be} values can be represented as

$$\frac{K_{\mathrm{be}}^{'}}{K_{\mathrm{be}}} \approx \frac{d_{\mathrm{b}}^{3/2}}{\left(d_{\mathrm{b}}^{'}\right)^{3/2}} \cdot \left(\frac{u_{\mathrm{b}}^{'}}{u_{\mathrm{b}}}\right)^{1/2} \tag{7}$$

with u_{b} estimated by [64]

$$u_{\mathrm{b}} = u_0 + 0.711\sqrt{g d_{\mathrm{b}}} \tag{8}$$

(with u_{mf} omitted). The bubble diameter can be estimated by the bubble fraction in the bed via

$$\delta_{\mathrm{b}} \approx \frac{u_0}{u_{\mathrm{b}}} = \frac{u_0}{u_0 + 0.711\sqrt{g d_{\mathrm{b}}}}, \tag{9}$$

i.e.

$$u_{\mathrm{b}} = \frac{u_0}{\delta_{\mathrm{b}}}, \tag{10}$$

$$d_{\mathrm{b}} = \frac{1}{g}\left[\frac{u_0\left(1-\delta_{\mathrm{b}}\right)}{0.711\delta_{\mathrm{b}}}\right]^2. \tag{11}$$

Substituting Eqs. (10) and (11) into Eq. (7) gives rise to

$$\frac{K_{\mathrm{be}}^{'}}{K_{\mathrm{be}}} = \left[\frac{\left(\delta_{\mathrm{b}}^{'}\right)^{2.5}}{\left(1-\delta_{\mathrm{b}}^{'}\right)^3}\right] \Bigg/ \left[\frac{\delta_{\mathrm{b}}^{2.5}}{\left(1-\delta_{\mathrm{b}}\right)^3}\right] \tag{12}$$

Figure 21 shows the computed ratios of K_{be} in BFB and FFB. It can be seen that $K^{'}_{\mathrm{be}}/K_{\mathrm{be}}$ are quite scattered, but they are in the range from 2.7 to 7.4, clearly demonstrating the improved gas-solids contacting due to the new baffles. In an industrial FCC regenerator, its static bed height and bed diameter will be larger than in our experimental column, but the fine content will be much higher (~20 wt% [7]) than in this study. This makes the accurate prediction of K_{be} in industrial FCC regenerators difficult. Therefore, we use $K^{'}_{\mathrm{be}}/ K_{\mathrm{be}}$ as an adjustable parameter in this baffled regenerator model to discuss the possible effect of the new baffles on the performance of an FCC regenerator.

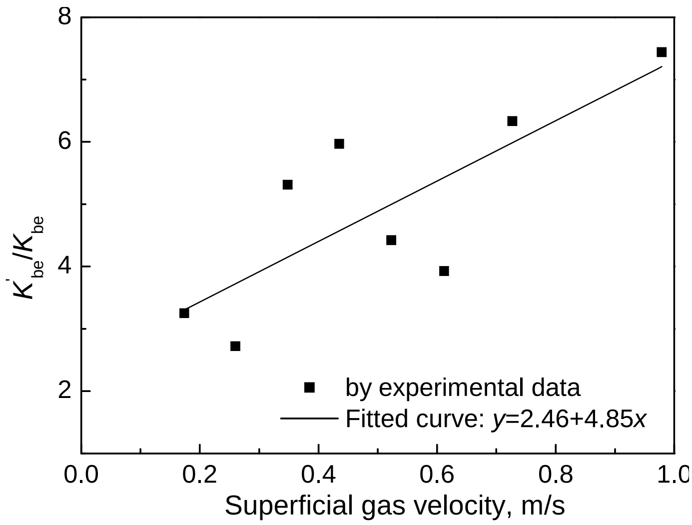

Fig. 21 Effect of the new baffles on the interphase mass transfer coefficient

(b) Solids exchange rate across the baffle layer

The solids exchange rate across the baffle layer in this study can be estimated by the backmixing suppression index, i.e.

$$F_{s,12} = (1 - I_{BMS}) F_{s,FFB} A_{t1}, \tag{13}$$

where $F_{s,FFB}$ is the internally circulating flux in a baffle-free fluidized bed. This is estimated here by an equation proposed by Geldart:[65]

$$F_{s,FFB} = \rho_p (1 - \varepsilon_{mf})(u_1 - u_{mf}) Y (\beta_w + 0.38\beta_d). \tag{14}$$

Here, u_1 is the superficial gas velocity in the dense bed of a regenerator.

For round catalyst particles, Baeyens and Geldart suggested:[66]

$$\beta_w = 0.43;\ \beta_d = 1.00;\ Y = 1.00. \tag{15}$$

The experimental I_{BMS} data of BFB in Fig. 18 can be correlated by

$$I_{\mathrm{BMS}} = -0.0318u_0^2 + 0.1273u_0 + 0.8729. \quad (16)$$

Then, substituting Eqs. (14) and (16) to Eq. (13) allows $F_{\mathrm{s,12}}$ to be estimated.

4.1.4 Mass balance

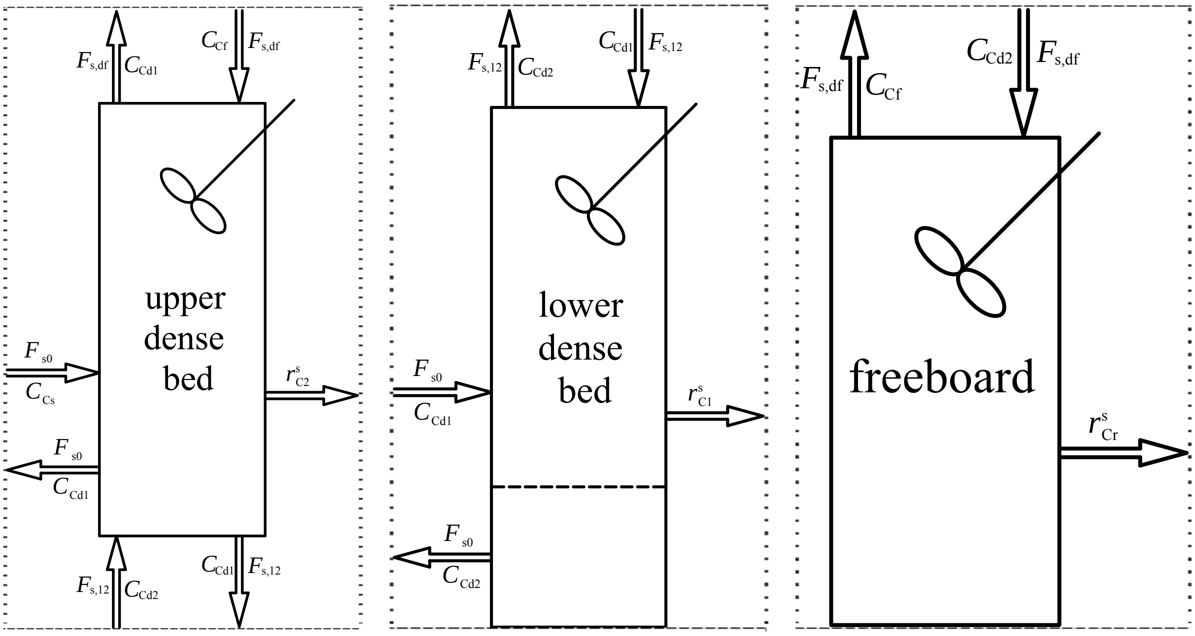

(a) upper dense bed (b) lower dense bed (c) freeboard

Fig. 22 Carbon balance in different regions of the baffled regenerator

The mass balance for gas components in the baffled regenerator model follows essentially the same method as for the baffle-free regenerator model.[24] Therefore, these contents are omitted in this paper. However, the carbon balance differs because of the different solids flow pattern employed. The carbon balance in different regions of the baffled regenerator can be represented schematically in Fig. 22. Following similar method to arrange the equations of carbon balance,[24] the carbon contents in the lower dense bed, upper dense bed and freeboard can be calculated subsequently.

$$C_{\mathrm{Cd2}} = C_{\mathrm{Cs}} - \frac{1200N_{\mathrm{ft}}}{F_{s0}}\left(y_{\mathrm{CO_2},z=H_{\mathrm{t}}} + y_{\mathrm{CO},z=H_{\mathrm{t}}}\right). \quad (17)$$

$$C_{\mathrm{Cd1}} = \frac{F_{s0}C_{\mathrm{Cs}} + F_{\mathrm{s,12}}C_{\mathrm{Cd2}} - 1200\left[N_{\mathrm{ft}}\left(y_{\mathrm{CO_2},z=H_{\mathrm{t}}} + y_{\mathrm{CO},z=H_{\mathrm{t}}}\right) - N_{\mathrm{dt}}\left(y_{\mathrm{CO_2},z=H_{\mathrm{l}}} + y_{\mathrm{CO},z=H_{\mathrm{l}}}\right)\right]}{\left(F_{\mathrm{s,12}} + F_{s0}\right)} \quad (18)$$

$$C_{\mathrm{Cf}}=C_{\mathrm{Cd1}}-\frac{1200N_{\mathrm{ft}}}{F_{\mathrm{s,df}}}\left[\left(y_{\mathrm{CO_2},z=H_{\mathrm{t}}}-y_{\mathrm{CO_2},z=H_{\mathrm{f}}^{+}}\right)+\left(y_{\mathrm{CO},z=H_{\mathrm{t}}}-y_{\mathrm{CO},z=H_{\mathrm{f}}^{+}}\right)\right]. \tag{19}$$

4.1.5 Heat balance

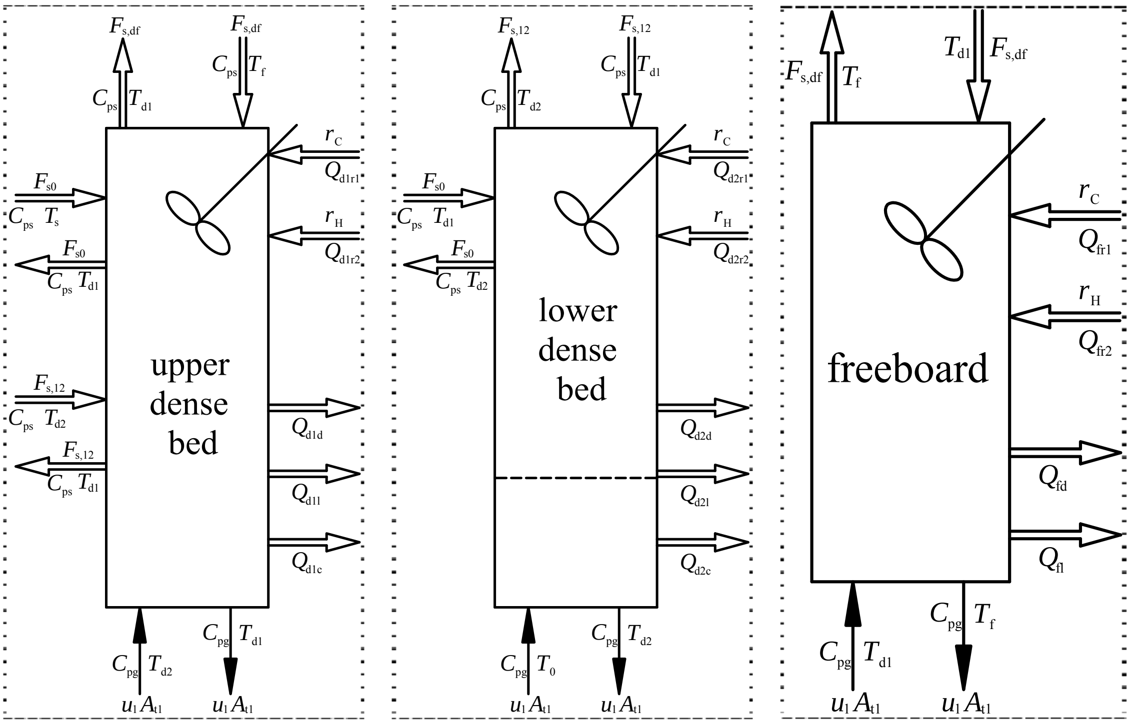

(a) upper dense bed (b) lower dense bed (c) freeboard

Fig. 23 Heat balance in different regions of the baffled regenerator

The heat balance in the baffled regenerator also need to consider the three regions as carbon mass balance. Nine and eight heat transfer items are considered and determined as our previous baffle-free regenerator model[24] in the lower and upper dense beds, respectively. The difference lies in an additional heat transfer item, i.e. heat removed by catalyst coolers, set to from the lower dense bed. This is to consider the potential advantage for higher catalyst-to-oil ratio. In freeboard, the same six heat transfer items are considered and determined. The heat balance in different regions of the baffled regenerator can be represented schematically in Fig. 23 and can be expressed in the following three equations,

$$\begin{aligned}&Q_{\mathrm{d1r1}}+Q_{\mathrm{d1r2}}+F_{\mathrm{s,df}}C_{\mathrm{ps}}\left(T_{\mathrm{f}}-T_{\mathrm{d1}}\right)+F_{\mathrm{s0}}C_{\mathrm{ps}}\left(T_{\mathrm{s}}-T_{\mathrm{d1}}\right)\\&\quad+F_{\mathrm{s,12}}C_{\mathrm{ps}}\left(T_{\mathrm{d2}}-T_{\mathrm{d1}}\right)+u_1A_{\mathrm{t1}}\rho_{\mathrm{g}}C_{\mathrm{pg}}\left(T_{\mathrm{d2}}-T_{\mathrm{d1}}\right)-\left(Q_{\mathrm{d1d}}+Q_{\mathrm{d1l}}+Q_{\mathrm{d1c}}\right)=0\end{aligned}, \tag{20}$$

$$Q_{\mathrm{d2r1}}+Q_{\mathrm{d2r2}}+F_{\mathrm{s,12}}C_{\mathrm{ps}}\left(T_{\mathrm{d1}}-T_{\mathrm{d2}}\right)+F_{\mathrm{s0}}C_{\mathrm{ps}}\left(T_{\mathrm{d1}}-T_{\mathrm{d2}}\right) \\ +u_1A_{\mathrm{t1}}\rho_{\mathrm{g}}C_{\mathrm{pg}}\left(T_0-T_{\mathrm{d2}}\right)-\left(Q_{\mathrm{d2d}}+Q_{\mathrm{d2l}}+Q_{\mathrm{d2c}}\right)=0, \tag{21}$$

$$Q_{\mathrm{fr1}}+Q_{\mathrm{fr2}}+F_{\mathrm{s,df}}C_{\mathrm{ps}}\left(T_{\mathrm{d1}}-T_{\mathrm{f}}\right)+u_2A_{\mathrm{t2}}\rho_{\mathrm{g}}C_{\mathrm{pg}}\left(T_{\mathrm{d1}}-T_{\mathrm{f}}\right)-\left(Q_{\mathrm{fd}}+Q_{\mathrm{fl}}\right)=0. \tag{22}$$

Let

$$Q_{\mathrm{Cd2}}=\left(Q_{\mathrm{d2r1}}+Q_{\mathrm{d2r2}}\right)-\left(Q_{\mathrm{d2d}}+Q_{\mathrm{d2l}}+Q_{\mathrm{d2c}}\right), \tag{23}$$

$$B_{\mathrm{Cd2}}=\left(F_{\mathrm{s,12}}+F_{\mathrm{s0}}\right)C_{\mathrm{ps}}+u_1A_{\mathrm{t1}}\rho_{\mathrm{g}}C_{\mathrm{pg}}, \tag{24}$$

Eq. (20) can then be arranged to give

$$T_{\mathrm{d1}}=\frac{B_{\mathrm{Cd2}}T_{\mathrm{d2}}-Q_{\mathrm{Cd2}}-u_1A_{\mathrm{t1}}\rho_{\mathrm{g}}C_{\mathrm{pg}}T_0}{\left(F_{\mathrm{s,12}}+F_{\mathrm{s0}}\right)C_{\mathrm{ps}}}. \tag{25}$$

Similarly, if we define

$$Q_{\mathrm{Cf}}=\left(Q_{\mathrm{fr1}}+Q_{\mathrm{fr2}}\right)-\left(Q_{\mathrm{fd}}+Q_{\mathrm{fl}}\right), \tag{26}$$

$$B_{\mathrm{Cf}}=F_{\mathrm{s,df}}C_{\mathrm{ps}}+u_2A_{\mathrm{t2}}\rho_{\mathrm{g}}C_{\mathrm{pg}}, \tag{27}$$

Eq. (22) can be arranged to give

$$T_{\mathrm{f}}=T_{\mathrm{d1}}+\frac{Q_{\mathrm{Cf}}}{B_{\mathrm{Cf}}}. \tag{28}$$

Finally, defining

$$Q_{\mathrm{Cd1}}=\left(Q_{\mathrm{d1r1}}+Q_{\mathrm{d1r2}}\right)-\left(Q_{\mathrm{d1d}}+Q_{\mathrm{d1l}}+Q_{\mathrm{d1c}}\right) \tag{29}$$

and combining Eqs. (20), (21) and (22) yields

$$Q_{\mathrm{Cf}} + Q_{\mathrm{Cd1}} + Q_{\mathrm{Cd2}} + F_{\mathrm{s0}} C_{\mathrm{ps}} \left(T_{\mathrm{s}} - T_{\mathrm{d2}} \right) + u_1 A_{\mathrm{t1}} \rho_{\mathrm{g}} C_{\mathrm{pg}} \left(T_0 - T_{\mathrm{f}} \right) = 0 \tag{30}$$

Combining Eqs. (25), (28) and (30) gives

$$\begin{aligned} & Q_{\mathrm{Cf}} + Q_{\mathrm{Cd1}} + Q_{\mathrm{Cd2}} + F_{\mathrm{s0}} C_{\mathrm{ps}} T_{\mathrm{s}} + u_1 A_{\mathrm{t1}} \rho_{\mathrm{g}} C_{\mathrm{pg}} \left(T_0 + \frac{Q_{\mathrm{Cd2}} + u_1 A_{\mathrm{t1}} \rho_{\mathrm{g}} C_{\mathrm{pg}} T_0}{\left(F_{\mathrm{s,12}} + F_{\mathrm{s0}} \right) C_{\mathrm{ps}}} + \frac{Q_{\mathrm{Cf}}}{B_{\mathrm{Cf}}} \right) \\ & = \left[F_{\mathrm{s0}} C_{\mathrm{ps}} + u_1 A_{\mathrm{t1}} \rho_{\mathrm{g}} C_{\mathrm{pg}} \frac{B_{\mathrm{Cd2}}}{\left(F_{\mathrm{s,12}} + F_{\mathrm{s0}} \right) C_{\mathrm{ps}}} \right] T_{\mathrm{d2}} \end{aligned}, \tag{31}$$

Here, the temperature of the lower dense bed, T_{d2}, is the only variable, and hence can be calculated. With T_{d2} known, T_{d1} and T_{f} can then be calculated by Eqs. (25) and (28), respectively.

4.2 Modeling results and discussion

4.2.1 Effect of solids backmixing suppression and gas-solids contacting improvement

Table 3 Effects of baffles on carbon content in regenerated catalysts

	Base	Case 1	Case 2	Case 3	Case 4
$K_{\mathrm{be}}/K_{\mathrm{be0}}$	1	1	2	2	3
I_{BMS}	0	0.96*	0	0.96*	0.96*
H_1/H_{f}	-	0.5	0.5	0.5	0.5
Q/Q_0	1	1	1	1	1
$M_{\mathrm{s}}/M_{\mathrm{s0}}$	1	1	1	1	1
F_{s0}, kg/s	381	381	381	381	381
P_{t}, $10^5 \times$ Pa	2.93	2.93	2.93	2.93	2.93
C_{Cs}, wt%	1.49	1.49	1.49	1.49	1.49
C_{Cr}, wt%	0.18	0.12	0.05	0.03	0.01

* calculated by Eq. (17).

The baffled regenerator model follows similar solution algorithm to the baffle-free regenerator model [24] to obtain the final solution. Similar flow chart and same model parameters as listed in the Table 2 of Zhang et al.[24] are again used to test the baffled regenerator model. However, this model cannot be compared with commercial data, because there is still no application of the new baffles in industrial FCC regenerators. There are also no industrial data available for other applied baffled regenerators. Therefore, this baffled regenerator model serves as a tool here to predict the effect of the new baffles in industrial FCC regenerators based on the experimental results obtained in the large cold model experiments of this study.

Table 3 lists the predicted effect of baffles in a FCC regenerator. Here, the base case is the incomplete regeneration mode in Zhang et al.[24] In Case 1, the effect of solids backmixing suppression is shown, with the value of I_{BMS} calculated by Eq. (16). C_{Cr} is predicted to decrease from 0.18 wt% to 0.12 wt% as a result of the reduction of solids exchange flux. Case 2 shows the effect of the improved gas-solids contacting. As can be seen, a doubled K_{be} can greatly improve the regeneration performance, reducing C_{Cr} from 0.18 wt% to 0.05 wt%. In Cases 3 and 4, the predicted effect of the combination of solids backmixing suppression and gas-solids contacting improvement is shown. C_{Cr} further decreases to lower levels. To consider the possible better fluidization quality in industrial FCC regenerators due to the larger gas viscosity and higher required fine contents than in the large cold model of this study, the increased K_{be}s listed in Table 3 are all conservative estimations for the baffle's effect in an industrial regenerator, as compared to the data in Fig. 21. Despite of the conservative estimations on baffle's improvement on gas-solids contacting, the modeled results indicate remarkable improvements in the performance of regenerators.

Table 4 Effect of baffles on operating parameters of FCC regenerators

	Base	Case 1	Case 2	Case 3	Case 4
K_{be}/K_{be0}	1	1	2	2	3
I_{BMS}	0	0.96*	0	0.96*	0.96*
H_l/H_f	-	0.5	0.5	0.5	0.5
Q/Q_0	1.25	1.045	1	1	1
M_s/M_{s0}	1	1	1	0.86	0.575
F_{s0}, kg/s	381	381	381	381	381
P_t, $10^5\times$Pa	2.93	2.93	2.93	2.93	2.93
C_{Cs}, wt%	1.49	1.49	1.49	1.49	1.49
C_{Cr}, wt%	0.05	0.05	0.05	0.05	0.05

* calculated by Eq. (17).

Table 4 adopts a different way for regenerator performance comparison. Here, the carbon content in the regenerated catalysts is fixed at 0.05 wt% for all cases. Except for air flow rate and solids inventory, all cases adopt the same operating parameters as the incomplete regeneration mode in Zhang et al.[24] The base case is also the baffle-free regenerator, but the air flow rate increases by 25% to provide the C_{Cr} of 0.05 wt%. It can be seen from Case 1 that only a slight increase of 4.5% in air flow rate can reduce the C_{Cr} to 0.05 wt% if the solids backmixing flux decreases by 96%.This means a saving of air flow rate of 16%. Case 2 shows that a small increase of K_{be}/K_{be0} from 1 to 2 can also reduce the C_{Cr} from 0.18 wt% to 0.05 wt%. This leads to a 20% reduction of the air flow rate. Cases 3 and 4 show that, if the solids backmixing flux maintains the same as Case 1, solids inventory can further decrease by 14% and 42.5% for K_{be}/K_{be0} of 2 and 3, respectively, on the base of 25% reduction of air flow rate.

In summary, the application of the new baffles in industrial FCC regenerators could bring significant improvement on their performance, resulting in major economic benefits. Further industrial experiments should be carried out to confirm quantitatively the actual effect of baffles. Moreover, it can be inferred from the modeled results that improving the gas-solids contacting is more effective than suppressing solids backmixing in improve FCC regenerator performance.

4.2.2 Effect of baffle level

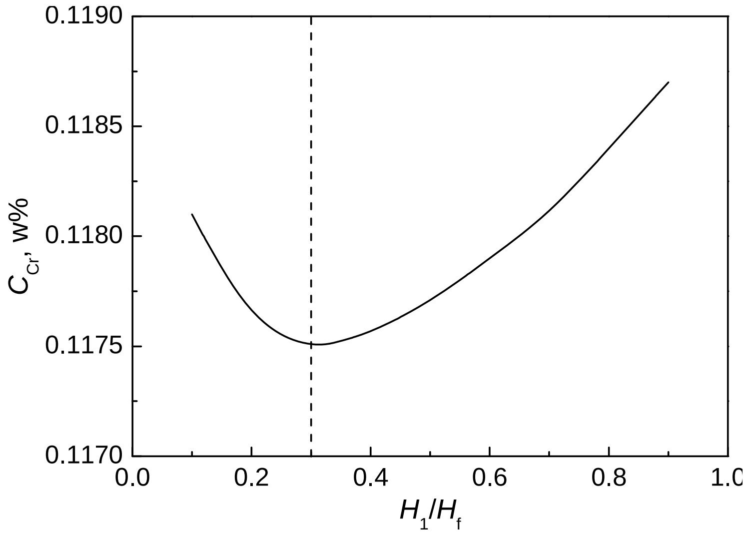

Fig. 24 Effect of baffle level on carbon content in regenerated catalysts (I_{BMS}=0.96; K_{be}/K_{be0}=1)

The baffle level can influence the performance of a FCC regenerator, because it determines the solids inventories in the two stages. Two examples are used here to demonstrate the effect of the baffle level. First, Take Case 1 in Table 3 for example, the effect of baffle level on C_{Cr} is shown in Fig. 24. In this case, baffle level is predicted to show a very small influence on C_{Cr}, with C_{Cr} reaching a minimum at $H_1/H_f \approx 0.3$, where the fractions of coke burned in the lower and upper dense beds are 47.5% and 45.4%, nearly equal. Second, for Case 3 in Table3 as another example, the effect of baffle level on C_{Cr}, as shown in Fig. 25, is much stronger than for Case 1. Here, C_{Cr} reaches a minimum at $H_1/H_f \approx 0.14$, where the fractions of coke burned in the lower and upper dense beds are 19% and 81%, respectively. In their patent of a parallel multistage FCC regenerator, Pfeiffer et al.[67] stated that the effect of multistage regenerators is more pronounced when a lower C_{Cr} is required and a 80~ 85% fraction of carbon burned in the first stage is the optimum partition if C_{Cr} is required to be less than 0.1 wt%. The results in Figs. 24 and 25 seem to be consistent with their conclusions.

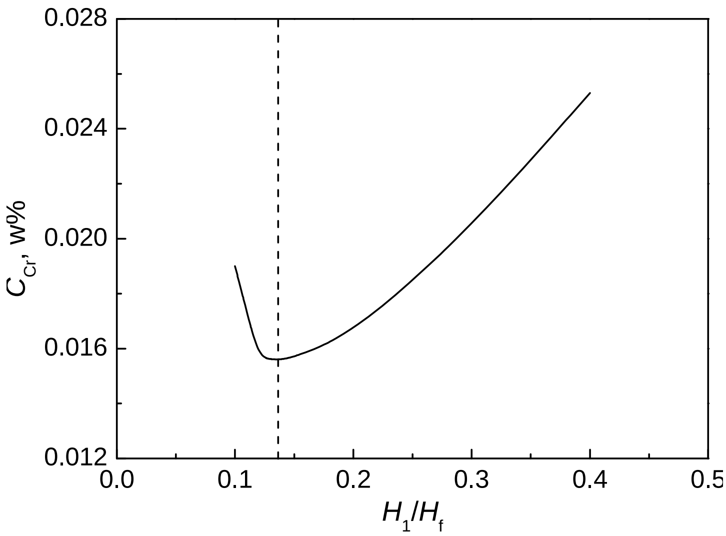

Fig. 25 Effect of baffle level on carbon content in regenerated catalysts (I_{BMS}=0.96; K_{be}/K_{be0}=2)

4.2.3 Predicted axial profiles of main hydrodynamic and reaction parameters

Figure 26 shows the predicted axial profiles of main hydrodynamic and reaction parameters in the baffled regenerator for an optimized operating condition (H_1/H_f=0.14; I_{BMS}=0.96; K_{be}/K_{be0}=2). The profile of voidage (see Fig. 26 (a)) is the same as for the baffle-free regenerator. There are temperature gradients among the lower dense bed, the upper dense bed and the freeboard, as shown in Fig. 26 (b). The temperature in the lower dense bed is 33 K lower than that in the upper dense bed. This is because all the heat removed by catalyst coolers is set to be from the lower dense bed, which helps to increase the ratio of catalyst to oil. The product yield and selectivity of catalytic cracking reactions can thus be enhanced due to the increased catalyst/oil ratio.

In Fig. 26 (c), the profiles of gas components are shown. The different gas component profiles in different regions can be explained by Table 5, where the properties of each region in the baffled regenerator are listed. In the grid region of the lower dense bed, the mass transfer constant is far larger than the reaction constant, so the reaction kinetics is the controlling factor. This leads to high oxygen concentration in the emulsion phase comparable to that in the dilute phase, resulting in a very high CBI in the grid region. In the bubbling region of the lower dense bed, mass transfer and reaction constants are of similar magnitude, so they both play important roles. The oxygen concentration in the emulsion phase is only slightly smaller than in the bubble phase, also leading to relatively high CBI in spite of the relatively low carbon content (see Fig. 26(d)). In the upper dense bed, the reaction constant is much larger than the mass transfer constant, showing the controlling role of mass transfer. Therefore, the oxygen concentration in the emulsion phase is far smaller than in the bubble phase. However, because of the higher carbon content (see Fig. 26 (d)), the CBI in this region is only slightly smaller than in the bubbling region of the lower dense bed. In the freeboard, all the oxygen has already been exhausted, so there is no carbon combustion and the carbon content in the freeboard is also equal to in the upper dense bed.

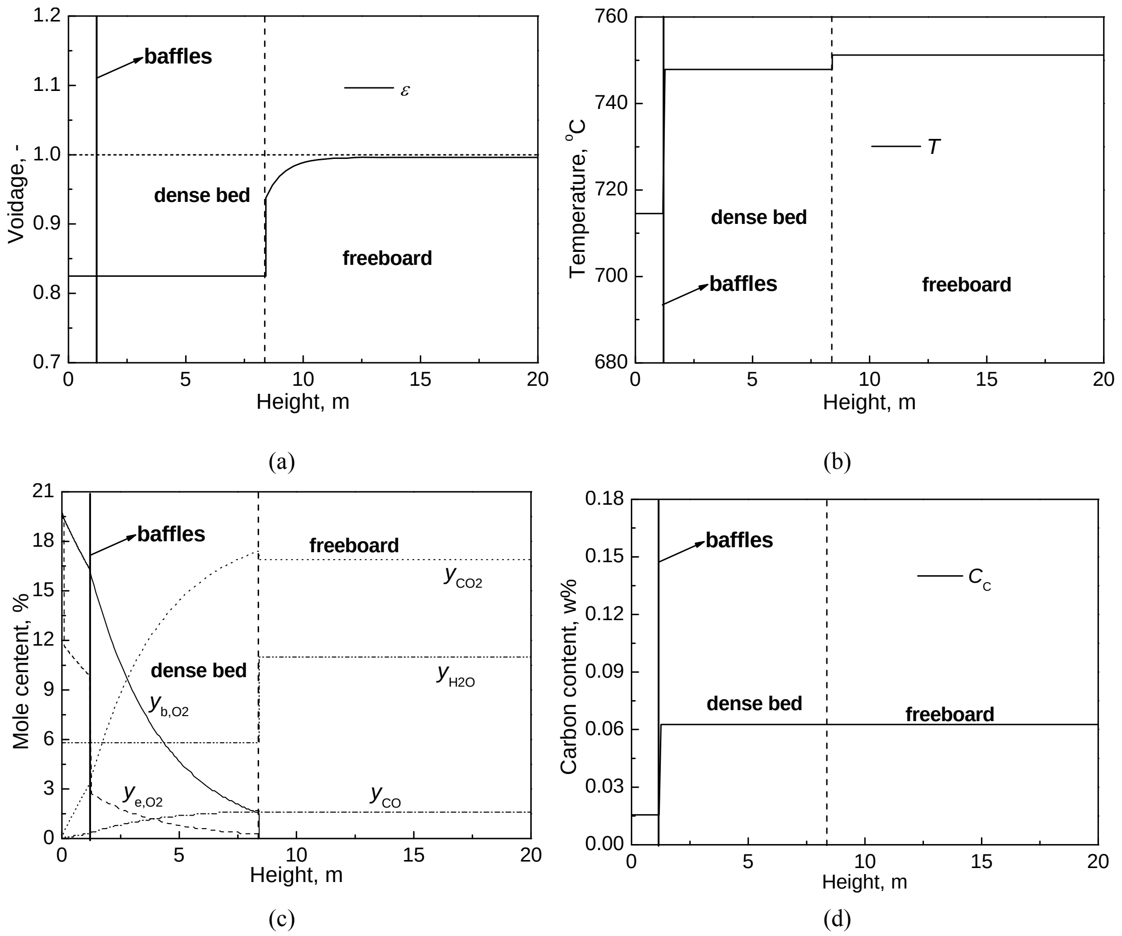

Fig. 26 Predicted profiles of (a) voidage, (b) temperature, (c) gas composition, and (d) carbon content for baffled FCC regenerator (H_1/H_f=0.14; I_{BMS}=0.96; K_{be}/K_{be0}=2).

In summary, the countercurrent baffled regenerator is predicted to provide relatively more uniform combustion intensities throughout the bed, with higher oxygen concentration and lower carbon content in the lower dense bed and lower oxygen concentration and higher carbon content in the upper dense bed. This should help increase the global carbon conversion and provide lower carbon content in the regenerated catalyst.

Table 5 Predicted properties of each region in a baffled FCC regenerator

	Lower dense bed		Upper dense bed	freeboard
	grid	bubbling		
Inventory fraction, %	0.9	11.7	77.5	9.9
Fraction of carbon combusted, %	2.3	16.7	81.0	0
CBI, kg/(h. ton (cat.))	281	155	114	0
Reaction constant*, 1/s	0.24	0.24	1.74	-
Mass transfer constant*, 1/s	26.68	0.36	0.36	-

*Details of the definitions can refer to Zhang et al.[24]

4.2.4 Other engineering concerns

Despite of these possible advantages, further industrial applications are still needed to validate its actual effects. Otherwise, there are also some possible downside concerns arising with adding baffles. Will the baffles bring additional pressure drop that may influence negatively the stability of particle flow or disturb the pressure balance of particle circulations. Due to the large open area ratio of the new baffle, the local gas velocity in the baffled height is only slightly higher than other baffle-free regions, resulting in a small decrease in local pressure drop. This may cause a slight decrease in the driving part of the regenerator-side solids circulation loop. Even when problems of low circulation rate arise, it can be easily corrected by increasing a small fraction of solids inventory in regenerator. Despite strong suppression of axial solids mixing, the cross-baffle solids circulation rate, which depends on the baffles' open area ratio and the superficial gas velocity, can still be maintained an order higher than the net solids circulation rate between reactor and regenerator. Therefore, the stability of particle flow in the baffled regenerator will not be a problem.

Will the baffles suffer serious erosion in the regenerator? The answer is probably no. According to previous studies,[68, 69] surface erosion rate by solids particles is usually proportional to 2.5~3.5 power of particle velocity. As the superficial gas velocity in a dense bed regenerator is no greater than 1.5 m/s, the adding of the new baffles will not increase particle velocity to a range comparable to in a FCC cyclone separator, where particle velocities can reach tens meters per second and anti-erosion measures must be taken.

The increased bed temperature gradient induced the added baffles, a result of solids backmixing suppression by baffles, could be a downside problem that needs to consider seriously. When a baffle layer is inserted into a regenerator, the bed temperature above the baffle, if there is no catalyst cooler, will decrease due to the staging effect of the baffle. The bed temperature beneath the baffle will keep constant if the carbon content in regenerated catalyst is the same, because it is only a function of unit heat balance. The extent of the temperature decrease depends on the baffle location and the cross-baffle solids circulation rate. A higher baffle position results in lower bed temperature above the baffle while higher cross-baffle solids circulation rate reduces the temperature gradient. According to the coke burning kinetics,[24] decrease in bed temperature will reduce the coke burning rate and the regenerator's efficiency. If the temperature is reduced lower than the firing point of coke, the dense bed region above the baffle layer will lose its regeneration function. Therefore, only one or two baffle layers are suggested in industrial designs. Moreover, baffles layer positions should be in the middle or lower positions of the dense bed. The predicted lower temperature beneath the baffle in Fig. 26(b) is actually due to that all surplus heat removed by the external catalyst cooler is set at the lower dense bed. To keep a better temperature gradient, an optimization can be done on the proportion of heat removed from the two regions.

According to our previous study,[26] the vane angle of the new baffle is a sensitive parameter and has an important effect on the bed hydrodynamic properties and gas-solids contacting. Therefore, stiffness design of the new baffle will be an important engineering issue that much be considered. If a layer of baffle bends during usage, some vane angles will deviate from the optimized design value, resulting in damage of its intensification effects and other unexpected downside effects. An industrial FCC regenerator is usually very large, sometimes with a diameter greater than ten meters, and operating at high temperature near 700^{o}C. Moreover, as an internal of FCC unit, it must withstand at least 3~5 years' working age. Therefore, engineering solutions must be found to guarantee its stiffness to cope with the long span, high working temperature and age demand.

5 Conclusions

In this study, a new multilayer baffle for intensifying the performance of FCC regenerators was proposed. Its effects on hydrodynamics and gas/solids mixing in fluidized beds of FCC particles were investigated in a large cold column with comparable dimensions to industrial FCC regenerators. The experimental results indicated that:

1. Compared to small laboratory-scale fluidized beds with low static beds, the new baffles are more effective in improving gas-solids contacting, as can be seen the significantly reduced amplitudes of pressure fluctuations, increased bed expansion and reduced particle carryover in the baffled fluidized bed.

2. The new baffles can also greatly suppress the more vigorous backmixing of gas and solids in the large column of this study. After insertion of the new baffles, the internal solids circulation flux decreased by 89~96%.

3. Based on a previous baffle-free FCC regenerator model,[24] a two-stage baffled countercurrent FCC regenerator model is proposed by adding two aspects of baffle effects: improved gas-solids contacting and solids backmixing suppression. The dense bed is modeled as two CSTRs in series with interchanging solids. The solids interchange flux across baffle layers and the interphase mass transfer coefficient are estimated based on the experimental results obtained in the old model experiments of this study. The modeled results demonstrate the likely positive effects of the new baffles on improving FCC regenerator performance. Improvement of gas-solids contacting is predicted to be particularly important for improving the performance of FCC regenerators. The model results also suggest that baffles should be mounted in the lower part of the dense bed to further optimize a regenerator's performance.

Nomenclature

A_{t1}, A_{t2} = cross-sectional area of dense bed and freeboard (m^2)

B_{Cd1}, B_{Cd2} = constants of heat flux in the upper and lower stages of dense bed (kJ/(K.s))

B_{Cf} = constant of heat flux in freeboard (kJ/(K.s))

C_C = carbon content (wt%)

C_{Cd1}, C_{Cd2} = carbon content in the upper and lower stages of the dense bed (wt%)

C_{Cf} = carbon content in the freeboard (wt%)

C_{Cr} = carbon content in the regenerated catalyst (wt%)

C_{Cs} = carbon content in the spent catalyst (wt%)

C_{H2} = hydrogen concentration (%)

C_{HF} = hydrogen concentration measured from sample at the outlet of column (%)

C_{Hs} = hydrogen content in the spent catalyst (wt%)

C_{pg} = specific heat of gas (kJ/(K.kg))

C_{ps} = specific heat of solids (kJ/(K.kg))

CBI= coke burning intensity (kg/(h.ton))

d_b = bubble diameter (m)

d_t = column diameter (m)

$D_{a,g}$ = gas axial dispersion coefficient (m^2/s)

D_g = gas diffusivity (m^2/s)

F_{45} = fines content factor, fraction of fine particles with diameter less than 45 μm

F_{s0} = catalyst circulation rate between reactor and regenerator (kg/s)

$F_{s,df}$ = catalyst circulation rate between dense bed and freeboard (kg/s

$F_{s,FFB}$ = internal solids circulation flux in FFB (kg/s)

$F_{s,12}$ = particle backmixing circulation rate from lower to upper stage of the dense bed (kg/s)

g = gravitational acceleration (m/s)

H_1 = height of the lower stage of dense bed (m)

H_f = expanded bed height (m)

I_{BMS} = backmixing suppression index

I_{hetero} = heterogeneity index (Pa)

I_{homo} = homogeneity index

k_j = jet-to-emulsion mass transfer coefficient (kg/m^2.s)

K_{be} = bubble-to-emulsion mass transfer coefficient (1/s)

M_s = total solids inventory in bed (kg)

M_{s0} = base total solids inventory in bed (kg)

N_{dt} = total gas molar flow rate in dense bed (kmol/s)

N_{ft} = total gas molar flow rate in freeboard (kmol/s)

P_t = pressure of in the top of a FCC regenerator (Pa)

Q = air volumetric flow rate (m^3/s)

Q_0 = base air volumetric flow rate (m^3/s)

Q_{Cd1}, Q_{Cd2} = heat flux constants in the upper and lower stages of dense bed (kJ/s)

Q_{Cf} = heat flux constant in freeboard (kJ/s)

Q_{d1c}, Q_{d2c} = heat release fluxes in the upper and lower stages of the dense bed due to catalyst coolers (kJ/s)

Q_{d1d}, Q_{d2d} = coke desorption heat fluxes in the upper and lower stages of dense bed (kJ/s)

Q_{d1l}, Q_{d2l} = heat releasing flux due to outside shells of upper and lower stages of dense bed (kJ/s)

Q_{d1r1}, Q_{d2r1} = heat released due to combustion of carbon in upper and lower stages of dense bed (kJ/s)

Q_{d1r2}, Q_{d2r2} = heat released due to combustion of hydrogen in upper and lower stages of dense bed (kJ/s)

Q_{fd} =coke desorption heat flux in freeboard (kJ/s)

Q_{fl} =heat releasing flux due to outside shell of freeboard (kJ/s)

Q_{fr1} = heat released due to combustion of carbon in freeboard (kJ/s)

Q_{fr2} = heat released due to combustion of hydrogen in freeboard (kJ/s)

r = radial coordinate (m)

R_c = radii of the column (m)

T = temperature (K)

T_0 = temperature of main air (K)

T_{d1} , T_{d2} = temperatures in upper and lower stages of dense bed (K)

T_f = temperature in freeboard (K)

T_s = temperature of spent catalysts (K)

u_0 = superficial gas velocity (m/s)

u_1 , u_2 = gas velocities in the dense bed and freeboard of a FCC regenerator (m/s)

u_b = bubble rise velocity (m/s)

u_{mf} = minimum fluidization velocity (m/s)

y = mole fraction of gas

Y = factor

z = axial coordinate (m)

Greek letters

β_w = volume fraction of wake

β_d = volume fraction of drift

δ_b = bubble volume fraction

Δh_j = axial distance of sampling tube from tracer gas injector (m)

ΔH_{CO} = heat released per kg of carbon combusted into CO (kJ/kg)

ΔH_{CO_2} = heat released per kg of carbon combusted into CO_2 (kJ/kg)

ΔH_{H_2O} = heat released per kg of hydrogen combusted into H_2O (kJ/kg)

ε = voidage

ε_{mf} = voidage at minimum fluidization velocity

ε_I ideal void fraction when bed expands homogeneously

π = circumference ratio

ρ_g = gas density (kg/m^3)

ρ_p = particle density (kg/m^3)

$\overline{\sigma_{dp}}$ = average standard deviation of differential pressure (Pa)

Subscripts

0 initial state

1 upper dense bed

2 lower dense bed

b bubble phase

d dense bed

f freeboard

g gas

j jet

mf minimum fluidization

out outlet

p particle

BFB baffled fluidized bed

CRC carbon content in regenerated catalyst

CSTR continuous stirred tank reactor

FFB baffle-free fluidized bed

References

(1) Henz, H.; Azevedo, F.; Chamberlain, O.; O'Connor, P., Re-invent fluid catalytic cracking. *Hydrocarbon Processing* **2004,** *83* (9), 41–48.

(2) Avidan, A. A.; Edwards, M.; Owen, H., Innovative improvements highlight FCC's past and future. *Oil & Gas Journal* **1990,** *88* (2), 33–58.

(3) Chen, Y.-M., Recent advances in FCC technology. *Powder Technol.* **2006,** *163* (1–2), 2–8.

(4) Reichle, A. D., Fluid catalytic cracking hits 50 year mark on the run. *Oil & Gas Journal* **1992,** *90* (20), 41–48.

(5) Chen, J., *Catalytic Cracking Process and Engineering (2ED)*. China Petrochemical Press: Beijing, China, 2005. (in Chinese)

(6) Sadeghbeigi, R., *Fluid Catalytic Cracking Handbook (3ED)*. Butterworth-Heinemann: Oxford, UK, 2012.

(7) Chen, J.; Cao, H.; Liu, T., Catalyst regeneration in fluid catalytic cracking. In *Advances in Chemical Engineering (Vol. 20): Fast Fluidization*, Kwauk, M., Ed. Academic Press London, UK, 2003; pp 389–419.

(8) Chen, Y.-M., Applications for fluid catalytic cracking. In *Handbook of Fluidization and Fluid-Particle Systems*, Yang, W.-C., Ed. Marcel Dekker, Inc.: New York, 2003; pp 379–396.

(9) Miller, R. B.; Yang, Y.-L.; Johnson, T. E., RegenMax™ technology: staged combustion in a single regenerator. *Proceeding of NPRA Annual Meeting* **1999,** *AM-99-14*.

(10) Miller, R. B.; Yang, Y.-L. Staged catalyst regeneration in a baffled fluidized bed. US Patent, 6,503,460, 2003.

(11) Sapre, A. V.; Leib, T. M.; Anderson, D. H., FCC Regenerator flow model. *Chem. Eng. Sci.* **1990,** *45* (8), 2203–2209.

(12) Jin, Y.; Yu, Z.; Zhang, L.; Yao, W.; Cai, P., Ridge type internal baffle for fluidized bed reactor. *Petrochemical Technology* **1986,** *15* (5), 269–277. (in Chinese)

(13) Jin, Y.; Yu, Z.; Zhang, L.; Shen, J.; Wang, Z., A study of pagoda type vertical internal baffle in gas-fluidized bed. *Journal of Chemical Industry and Engineering (China)* **1980,** *31* (2), 117–128. (in Chinese)

(14) Wang, Z.; Jin, Y.; Yao, W.; Yu, Z., Investigation on the turbulent fluidized bed reactor for vinyl acetate production in commercial scale. *Chemical Reaction Engineering and Technology* **1995,** *11* (1), 50–55. (in Chinese)

(15)Miller, R. B.; Yang, Y.-L.; Gbordzoe, E.; Johnson, D. L.; Mallo, T. A., New developments in FCC feed injection and stripping technologies. In *NPRA Annual Meeting*, San Antonio, Texas, USA, 2000; pp AM–00–08.

(16) Rall, R. R.; DeMulder, B., New internal for maximizing performance of FCC catalyst strippers. In *12th Annual Stone & Webster Refining Seminar*, San Francisco, California, USA, 2000.

(17) Harrison, D.; Grace, J. R., Fluidized beds with internal baffles. In *Fluidization*, Yang, W.-C., Ed. Academic Press: London and New York, 1971; pp 599–626.

(18) Jin, Y.; Wei, F.; Wang, Y., Effect of internal tubes and baffles. In *Handbook of Fluidization and Fluid-Particle Systems*, Yang, W.-C., Ed. Marcel Dekker, Inc.: New York, 2003; pp 171–200.

(19) Zhang, Z.; Tian, G., Development of the novel grid type multi-stage regeneration technology for FCC unit. *China Petroleum Processing and Petrochemical Technology* **2006,** *7* (2), 43–47.

(20) Hedrick, B. W. Three-stage counter-current FCC regenerator. US Patent, 7,915,191, 2011.

(21) Li, J.; Luo, G.; Wei, F., A multistage NOx reduction process for a FCC regenerator. *Chem. Eng. J.* **2011,** *173* (2), 296–302.

(22) Guigon, P.; Large, J. F.; Bergougnou, M. A., Application of the Kunii–Levenspiel model to a multistage baffled catalytic cracking regenerator. *The Chemical Engineering Journal* **1984,** *28* (3), 131–138.

(23) Lu, C.; Zhang, Y. A new internal for gas-solid fluidized beds. Chinese Patent, 200610114153.4, 2006.

(in Chinese)

(24) Zhang, Y.; Lu, C.; Li, T., A practical countercurrent fluid catalytic cracking regenerator model for in situ operation optimization. *AlChE J.* **2012,** *58* (9), 2770–2784.

(25) Zhang, Y. Hydrodynamics and mixing properties of a novel baffled fluidized bed. Doctoral dissertation, China University of Petroleum, Beijing, Beijing, China, 2009.

(26) Zhang, Y.; Lu, C.; Shi, M., Effects of structure parameters and arrangements of louver baffles on the hydrodynamics of turbulent fluidized beds of fine particles. *Petroleum Processing and Petrochemicals* **2007,** *38* (7), 64-69. (in Chinese)

(27) Zhang, Y.; Grace, J. R.; Bi, X.; Lu, C.; Shi, M., Effect of louver baffles on hydrodynamics and gas mixing in a fluidized bed of FCC particles. *Chem. Eng. Sci.* **2009,** *64* (14), 3270–3281.

(28) Zhang, Y.; Lu, C.; Grace, J. R.; Bi, X.; Shi, M., Gas back-mixing in a two-dimensional baffled turbulent fluidized bed. *Ind. Eng. Chem. Res.* **2008,** *47* (21), 8484–8491.

(29) Zhang, Y.; Lu, C.; Shi, M., Evaluating solids dispersion in fluidized beds of fine particles by gas backmixing experiments. *Chem. Eng. Res. Des.* **2009,** *87* (10), 1400–1408.

(30) Niccum, P. K.; Santner, C. R., KBR fluid catalytic cracking process. In *Handbook of Petroleum Refining Processes (3ED)*, Meyers, R. A., Ed. McGraw-Hill: New York, 2003.

(31) Zhang, Y.; Wang, H.; Chen, L.; Lu, C., Systematic investigation of particle segregation in binary fluidized beds with and without multilayer horizontal baffles. *Ind. Eng. Chem. Res.* **2012,** *51* (13), 5022–5036.

(32) Werther, J., Scale-up modeling for fluidized bed reactors. *Chem. Eng. Sci.* **1992,** *47* (9-11), 2457–2462.

(33) Clark, N. N.; Atkinson, C. M., Amplitude reduction and phase lag in fluidized-bed pressure measurements. *Chem. Eng. Sci.* **1988,** *43* (7), 1547–1557.

(34) Zhang, Y.; Lu, C.; Shi, M., A new homogeneity index to characterize the fluidization quality for non-slugging fluidized beds of Geldart A particles. *Powder Technol.* **2009,** *191* (1-2), 182–187.

(35) Roy, R.; Davidson, J. F. Similarity between gas-fluidized beds at elevated temperature and pressure, In *Fluidization VI*, New York, USA, Grace, J. R.; Shemilt, L. W.; Bergougnou, M. A., Eds. Engineering Foundation: New York, USA, 1989; pp 293–300.

(36) Darton, R. C.; Lanauze, R. D.; Davidson, J. F.; Harrison, D., Bubble growth due to coalescence in fluidized beds. *Transactions of the Institution of Chemical Engineers* **1977,** *55*, 274–280.

(37) Bi, H. T. Flow regime transitions in gas-solids fluidization and transport. Docteral dissertation, University of British Columbia, Vancouver, Canada, 1994.

(38) Zhang, Y.; Bi, H. T.; Grace, J. R.; Lu, C., Comparison of decoupling methods for analyzing pressure fluctuations in gas-fluidized beds. *AlChE J.* **2010,** *56* (4), 869–877.

(39) van Ommen, J. R.; Mudde, R. F. Measuring the gas-solids distribution in fluidized beds - a review, In *The 12th International Conference on Fluidization - New Horizons in Fluidization Engineering*, Vancouver, Canada, Berruti, F.; Bi, X.; Pugsley, T., Eds. Vancouver, Canada, 2007; pp 31–45.

(40) Deshmukh, S. A. R. K.; van Sint Annaland, M.; Kuipers, J. A. M., Gas back-mixing studies in membrane assisted bubbling fluidized beds. *Chem. Eng. Sci.* **2007,** *62* (15), 4095–4111.

(41) Liu, Y.; Lan, X.; Xu, C.; Wang, G.; Gao, J., CFD simulation of gas and solids mixing in FCC strippers. *AlChE J.* **2012,** *58* (4), 1119–1132.

(42) Nguyen, H. V.; Whitehead, A. B.; Potter, O. E., Gas backmixing, solids movement, and bubble activities in large scale fluidized beds. *AlChE J.* **1977,** *23* (6), 913–922.

(43) Zhang, Y.; Lu, C.; Shi, M., A practical method to estimate the bed height of a fluidized bed of fine particles. *Chem. Eng. Tech.* **2008,** *31* (12), 1735–1742.

(44) Bi, H. T.; Fan, L.-S., Existence of turbulent regime in gas-solid fluidization. *AlChE J.* **1992,** *38* (2), 297–301.

(45) Bi, H. T.; Grace, J. R., Effect of measurement method on the velocities used to demarcate the onset of turbulent fluidization. *The Chemical Engineering Journal and the Biochemical Engineering Journal* **1995,** *57* (3), 261–271.

(46) Cai, P.; Jin, Y.; Yu, Z.; Wang, Z., Mechanism of flow regime transition from bubbling to turbulent fluidization. *AlChE J.* **1990,** *36* (6), 955–956.

(47) Ellis, N.; Bi, H. T.; Lim, C. J.; Grace, J. R., Hydrodynamics of turbulent fluidized beds of different diameters. *Powder Technol.* **2004,** *141* (1–2), 124–136.

(48) Yerushalmi, J.; Cankurt, N. T.; Geldart, D.; Liss, B., Flow regimes in vertical gas-solid contact systems. *AlChE Symp. Ser.* **1978,** *174* (176), 1–12.

(49) Bi, H. T.; Ellis, N.; Abba, I. A.; Grace, J. R., A state-of-the-art review of gas-solid turbulent fluidization. *Chem. Eng. Sci.* **2000,** *55* (21), 4789–4825.

(50) Zhu, H.; Zhu, J., New investigation in regime transition from bubbling to turbulent fluidization. *Can. J. Chem. Eng.* **2008,** *86* (3), 553–562.

(51) Cai, P. The transition of flow regime in dense phase gas-solid fuidized bed. Doctoral dissertation, Tsinghua University, Beijing, China, 1989.

(52) Yerushalmi, J.; Cankurt, N. T., Further studies of the regimes of fluidization. *Powder Technol.* **1979,** *24* (2), 187–205.

(53) Wells, J. W., Streaming flow in large scale fluidization. In *AIChE Annual Meeting: Particle Technology Forum*, Reno, Nevada, USA , 2001.

(54) Karri, S. B. R.; Issangya, A.; Knowlton, T. M. Gas bypassing in deep fluidized beds, In *Fluidization XI – Present and Future for Fluidization Engineering*, Ischia, Italy, Arena, U.; Chirone, R.; Miccio, M.; Salatino, P., Eds. Ischia, Italy, 2004; pp 515–521.

(55) Issangya, A. S.; Knowlton, T.; Karri, S. B. R. Detection of gas bypassing due to jet streaming in deep fluidized beds of Group A particles, In *Fluidization XII - New Horizons in Fluidization Engineering*, Vancouver, Canada, Bi, H. T.; Pugsley, T., Eds. Vancouver, Canada, 2007; pp 775–782.

(56) Cocco, R.; Issangya, A.; Karri, S. B. R.; Knowlton, T., Understanding streaming flow in deep fluidized

beds. In *AIChE Annual Meeting: Particle Technology Forum.*, San Francisco, USA , 2006.

(57) Kunii, D.; Levenspiel, O., *Fluidization Engineering (2ED).* Butterworth-Heinemann: USA, 1991.

(58) Glicksman, L. R., Fluidized Bed Scale-up. In *Fluidization, Solids Handling, and Processing*, Wen-Ching, Y., Ed. William Andrew Publishing: Westwood, NJ, 1998; pp 1-110.

(59) Knowlton, T. M.; Karri, S. B. R.; Issangya, A., Scale-up of fluidized-bed hydrodynamics. *Powder Technol.* **2005,** *150* (2), 72–77.

(60) Chavarie, C.; Grace, J. R., Performance analysis of a fluidized bed reactor. I. visible flow behavior. *Ind. Eng. Chem. Funda.* **1975,** *14* (2), 75–79.

(61) Chavarie, C.; Grace, J. R., Performance analysis of a fluidized bed reactor. III. modification and extension of conventional two-phase models. *Ind. Eng. Chem. Funda.* **1981,** *14* (2), 86–91.

(62) Chavarie, C.; Grace, J. R., Performance analysis of a fluidized bed reactor. II. observed reactor behavior compared with simple two-phase models. *Ind. Eng. Chem. Funda.***1981,** *14* (2), 79–86.

(63) Sit, S. P.; Grace, J. R., Effect of bubble interaction on interphase mass transfer in gas fluidized beds. *Chem. Eng. Sci.* **1981,** *36* (2), 327–335.

(64) Davidson, J. F.; Harrison, D., *Fluidized particles*. Cambridge University Press: UK, 1963.

(65) Geldart, D., *Gas Fluidization Technology*. John Wiley & Sons: Chichester, UK, 1986.

(66) Baeyens, J.; Geldart, D., Fluidization and its applications. Toulouse, France. , 1973; p 182.

(67) Pfeiffer, R. W.; Bronxville, N. Y.; Garrett, L. W. Staged fluidized catalyst regeneration process. US Patent, 3,563,911, 1968.

(68) Finnie, I. Erosion of surfaces by solid particles. *Wear*. **1960**, 3, 87–103.

(69) Li, C. Y. ; Zakkay, V. Hydrodynamics and erosion modeling of fluidized-bed combustors. *J. Fluids Eng. Trans. ASME*. **1994**, 116, 746–755.